Received: 31 January 2022 | Accepted: 9 October 2023

DOI: 10.1111/mafi.12423

ORIGINAL ARTICLE

MATHEMATICAL FINANCE An International Journal of Mathematics, Statistics and Financial Economics

WILEY

Sig-Wasserstein GANs for conditional time series generation

Shujian Liao[1] | **Hao Ni**[1] | **Marc Sabate-Vidales**[2] | **Lukasz Szpruch**[2] | **Magnus Wiese**[3] | **Baoren Xiao**[1]

[1]University College London, London, UK

[2]University of Edinburgh, Edinburgh, UK

[3]University of Kaiserslautern, Kaiserslautern, Germany

Correspondence
Hao Ni, University College London, London, UK.
Email: h.ni@ucl.ac.uk

Funding information
Engineering and Physical Sciences Research Council, Grant/Award Numbers: EP/N510129/1, EP/S026347/1

Abstract

Generative adversarial networks (GANs) have been extremely successful in generating samples, from seemingly high-dimensional probability measures. However, these methods struggle to capture the temporal dependence of joint probability distributions induced by time-series data. Furthermore, long time-series data streams hugely increase the dimension of the target space, which may render generative modeling infeasible. To overcome these challenges, motivated by the autoregressive models in econometric, we are interested in the conditional distribution of future time series given the past information. We propose the generic conditional Sig-WGAN framework by integrating Wasserstein-GANs (WGANs) with mathematically principled and efficient path feature extraction called the signature of a path. The signature of a path is a graded sequence of statistics that provides a universal description for a stream of data, and its expected value characterizes the law of the time-series model. In particular, we develop the conditional Sig-W_1 metric that captures the conditional joint law of time series models and use it as a discriminator. The signature feature space enables the explicit

representation of the proposed discriminators, which alleviates the need for expensive training. We validate our method on both synthetic and empirical dataset and observe that our method consistently and significantly outperforms state-of-the-art benchmarks with respect to measures of similarity and predictive ability.

KEYWORDS
conditional generative adversarial networks, generative adversarial networks, rough path theory, time series modeling, Wasserstein generative adversarial networks

1 | INTRODUCTION

Ability to generate high-fidelity synthetic time-series datasets can facilitate testing and validation of data-driven products and enable data sharing by respecting the demand for privacy constraints (Assefa et al., 2020; Bellovin et al., 2019; Tucker et al., 2020). Until recently, time-series models were mostly conceived by handcrafting a parsimonious parametric model, which would best capture the desired statistical and structural properties or the so-called stylized facts of the time series data. Typical examples are discrete time autoregressive econometric models (Tsay, 2005), or continuous time stochastic differential equations (SDEs) (Karatzas & Shreve, 1998). In many applications, such as finance and economics, one cannot base models on well-established "physical laws" and the risk of handcrafting inappropriate models might be significant. It is, therefore, tempting to build upon success of nonparametric unsupervised learning method such as deep generative modeling (DGM) to enable data-driven model selection mechanisms for dynamically evolving data sets such as time-series. However, off-the-shelf DGMs perform poorly on the task of learning the temporal dynamics of multivariate time series data $x_{1:T} = (x_1, \dots, x_T) \in \mathbb{R}^{d\times T}$ due to (1) complex interaction between temporal features and spatial features, and (2) potential high dimension for the joint distribution of x (e.g., when $T >> 1$), see, for example, Mescheder et al. (2018).

In this work, we are interested in developing a data-driven nonparametric model for the conditional distribution $\mathrm{Law}(x_{\mathrm{future}}|x_{past})$ of future time series given $x_{\mathrm{past}} := x_{t-\bar{p}+1:t}$. This setting includes classical auto-regressive processes. Learning conditional distributions is particularly important in the cases of (1) predictive modeling: it can be directly used to forecast future time series distribution given the past information; (2) causal modeling: conditional generator can be used to produce counterfactual statements; and (3) building the joint law through conditional laws enables to incorporate a prior into the learning process, which is necessary for building high-fidelity generators.

Learning the conditional distribution is often more desirable than learning the joint law and can lead to more efficient learning with a smaller amount of data (Buehler et al., 2020; Ng & Jordan, 2002). To see that, consider the following example.

Example 1.1 (Auto regressive process). Let $Z_t \sim N(0, \Sigma)$ be d-dimensional Gaussian random variable. Fix $a : \mathbb{R}^{d\times\bar{p}} \times \mathbb{R}^d \to \mathbb{R}^d$. Define an auto-regressive process $(X_t)_{t\geq 0}$ with the initial condition

$X_{1:\bar{p}} = x_{1:\bar{p}}$, as $X_{t+1} = a(X_{t-\bar{p}+1:t}, Z_{t+1})$. Hence, one can see that

$$\mathrm{Law}(X_{1:T}) = \prod_t \mathrm{Law}(X_{t+1}|X_{t-\bar{p}+1:t}).$$

As a consequence, the problem of learning distribution over $\mathbb{R}^{d\times T}$ can be reduced to learning conditional distribution over $\mathbb{R}^d$.

In our setting, the conditional law is time invariant and hence having only one data trajectory $x_{1:T}$ gives $T - \bar{p} - 1$ samples. This should be contrasted with having one sample when trying to learn $\mathrm{Law}(X_{1:T})$ directly.

Structure

The problem of calibrating a generative model in the time series domain is formulated in Section 2. There we overview the key results of this work against the work available in literature. In Section 3, we introduce the signature of a path formally. In Section 4, we establish key theoretical results of this work. In Section 5, we present the algorithm while in Section 6, we present extensive numerical experiments.

2 | PROBLEM FORMULATION

Fix $T > 0$ and $X := (X_1, \dots, X_T) \in \mathbb{R}^{d\times T}$ is a d-dimensional time series of length T. Let W be the window size (typically $W << T$). Suppose that we have access to one realization of X, that is, $(x_1, \dots, x_T)$ and then obtain the N copies of time series segment of a window size W by sliding window. We assume that for each t, the time series segment $(x_{t+1} : \cdots, x_{t+W})$ is sampled from the same but *unknown* distribution on the time series (path) space $\mu \in \mathcal{P}(\mathbb{R}^{d\times W})$. The objective of the *unconditional* generative model is to train a generator such as to produce a $\mathbb{R}^{d\times W}$-valued random variable whose law is close to μ using time series data x.[1]

In contrast, this paper focuses on the task of the *conditional* generative model of future time series when conditioning on past time series. Let $\bar{p}, \bar{q}$ denote the window size of the past time series $X_{\mathrm{past},t} := (X_{t-\bar{p}+1}, \dots, X_t) \in \mathbb{R}^{d\times\bar{p}} =: \mathcal{X}$ and future time series $X_{\mathrm{future},t} := (X_{t+1}, \dots, X_{t+\bar{q}}) \in \mathbb{R}^{d\times\bar{q}} =: \mathcal{Y}$, respectively. Assume that the joint distribution of $(X_{\mathrm{future},t}, X_{\mathrm{past},t}) = (X_{t-\bar{p}+1,t+\bar{q}})$ does not depend on time t. Given a realization of time series $(x_1, \dots, x_T)$, at each time t, the pairs of past path $x_{\mathrm{past},t} := (x_{t-\bar{p}+1}, \dots, x_t) \in \mathcal{X}$ and future path $x_{\mathrm{future},t} := (x_{t+1}, \dots, x_{t+\bar{q}}) \in \mathcal{Y}$ are sampled from the same but *unknown* distribution of $\mathcal{X}\times\mathcal{Y}$-valued random variable, denoted by $(X_{\mathrm{past}}, X_{\mathrm{future}})$. We aim to train a generator to produce the conditional law, denoted by $\mu_t(x) := \mathrm{Law}(X_{\mathrm{future},t}|X_{\mathrm{past},t} = x)$. As $\mu_t(x)$ is independent with t and hence we write $\mu(x)$ for simplicity. But of course, the methodology developed here all applies if one can access a collection of $(X^{(i)}_{\mathrm{past}}, X^{(i)}_{\mathrm{future}})_{i=1}^N$ of N independent copies of the past and future time series for $N \geq 1$.

More specifically, the aim of the conditional generative model is to map samples from some basic distribution μ^Z supported on $\mathcal{Z} \subseteq \mathbb{R}^{d_z}$ together with data $x_{\mathrm{past},t}$ into samples from the conditional law $\mu(x_{\mathrm{past},t})$. Given latent $(\mathcal{Z}, \mathcal{B}(\mathcal{Z}))$, conditional $(\mathcal{X}, \mathcal{B}(\mathcal{X}))$ and target $(\mathcal{Y}, \mathcal{B}(\mathcal{Y}))$ measurable spaces, one considers a map $G : \Theta^{(g)} \times \mathcal{X} \times \mathcal{Z} \to \mathcal{Y}$, with $\Theta^{(g)}$ being a parameter space. Given parameters $\theta^{(g)} \in \Theta^{(g)}$ and $x_{\mathrm{past},t}$, $G(\theta^{(g)}, x_{\mathrm{past},t})$ transports μ_z into $\nu(\theta^{(g)}, x_{\mathrm{past},t}) := G(\theta^{(g)}, x_{\mathrm{past}})_{\#}\mu_z = \mu_z(G(\theta^{(g)}, x_{\mathrm{past},t})^{-1}(B))$, $B \in \mathcal{B}(\mathcal{Y})$. The aim is to find θ such that $\nu(\theta, X_{\mathrm{past},t})$

is a good approximation of $\mu(X_{\text{past},t})$ with respect to a suitable metric. Often the metric of choice is a Wasserstein distance, which leads to

$$\mathrm{W}_1\left(\mu(x_{\text{past}}), \nu(\theta^{(g)}, x_{\text{past}})\right) = \sup_{|f|_{\text{Lip}}\leq 1} \mathbb{E}_{\mu(x_{\text{past}})}[f(X_{\text{future}})] - \mathbb{E}_{\nu(\theta^{(g)}, x_{\text{past}})}[f(X_{\text{future}})] \tag{1}$$

The optimal transport metrics, such as Wasserstein distance, are attractive due to their ability to capture meaningful geometric features between measures even when their supports do not overlap, but are expensive to compute (Genevay et al., 2019). Furthermore, when computing Wasserstein distance for conditional laws, one needs to compute the conditional expectation $\mathbb{E}_{\mu(x_{\text{past}})}[f(X_{\text{future}})]$ using input data. In the continuous setting studied in this paper, this is computationally heavy and typically will introduce additional bias (e.g., due to employing least square regression to compute an approximation to the conditional expectation).

Since our aim is to learn the conditional law for all possible conditioning random variables, we consider

$$\mathbb{E}_{X_{\text{past}}\sim\mu}[\mathrm{W}_1\left(\mu(X_{\text{past}}), \nu(\theta, X_{\text{past}})\right)].$$

Note that, since W_1 is non-negative, $\mathbb{E}[\mathrm{W}_1(\mu(X_{\text{past}}), \nu(\theta, X_{\text{past}}))] = 0$ implies that $\mu(x_{\text{past}}) = \nu(\theta, x_{\text{past}})$ almost surely.

Challenges in implementing W_1-GAN for conditional laws

There are two key challenges when one aims to implement W_1-GAN for conditional laws.

Challenge 1: Min–max problem. A typical implementation of W_1-GAN would require introduction of a parametric function approximation $\Theta^{(d)} \times \mathcal{Y} \ni (\theta^{(d)}, \omega) \mapsto f(\theta^{(d)}, \omega)$ such that $\omega \mapsto f(\theta^{(d)}, \omega)$ is 1-Lip. In the case of neural network approximation, this can be achieved by clipping the weights or adding penalty that ensures $\nabla_\omega f(\theta^{(d)}, \omega)$ is less than 1, see Gulrajani et al. (2017). Recall a definition of W_1 in Equation (1) and define

$$\ell(\theta^{(g)}, \theta^{(d)}) := \mathbb{E}_{X_{\text{past}}\sim\mu}\left[\mathbb{E}_{\mu(X_{\text{past}})}\left[f(\theta^{(d)}, X_{\text{future}})\right] - \mathbb{E}_{\nu(\theta^{(g)}, X_{\text{past}})}\left[f(\theta^{(d)}, X_{\text{future}})\right]\right].$$

Training conditional W_1-GAN constitutes solving the min–max problem

$$\min_{\theta^{(g)}} \max_{\theta^{(d)}} \ell(\theta^{(g)}, \theta^{(d)}). \tag{2}$$

In practice, the min–max problem is solved by iterating gradient descent-ascent algorithms and its convergence can be studied using tools from game theory (Lin et al., 2020; Mazumdar et al., 2019). However, it is well known that the first order method, which is typically used in practice, might not converge even in the convex-concave case (Daskalakis et al., 2017; Daskalakis & Panageas, 2018; Mertikopoulos et al., 2018). Consequently, the adversarial training is notoriously difficult to tune (Farnia & Ozdaglar, 2020; Mazumdar et al., 2019), and generalization error is very sensitive to the choice of discriminator and hyper-parameters, as it was demonstrated in large scale study in Lucic et al. (2018).

Challenge 2: Computation of the conditional expectation. In addition to the challenge of solving a min–max for each new parameter $\theta^{(d)}$, one needs to compute the conditional expectation $\mathbb{E}_{\mu(X_{\text{past}})}[f(\theta^{(d)}, X_{\text{future}})]$ (or $\mathbb{E}_{\mu(X_{\text{past}})}[\nabla_{\theta^{(d)}} f(\theta^{(d)}, X_{\text{future}})]$ if one can interchange differentiation

and integration). From Doob–Dynkin lemma, we know that this conditional expectation is a measurable function of X_{past} and approximation of these is computationally heavy and can be recast as a mean-square optimization problem

$$\mathbb{E}\left[\left|f\left(\theta^{(d)}, X_{\text{future}}\right) - \mathbb{E}_{\mu(X_{\text{past}})}\left[f(\theta^{(d)}, X_{\text{future}})\right]\right|^2\right] = \inf_{h \text{ measurable}} \mathbb{E}\left[\left|f(\theta^{(d)}, X_{\text{future}}) - h(X_{\text{past}})\right|^2\right].$$

Practical solution of this problem requires an additional function approximation, which may introduce additional bias and makes the overall algorithm much harder to tune.

2.1 | Summary of the key results

Discrete time econometric models can be viewed as discretisation of certain SDEs type models (Klüppelberg et al., 2004). The continuous time perspective by embedding discrete time series into a path space, which we follow in this paper, is particularly useful when learning from irregularly sampled data sets and designing efficient training methods that naturally scale when working with high and ultra high frequency data (Cuchiero et al., 2020; Gierjatowicz et al., 2022; Liu et al., 2019). Our approach utilizes the signature of a path, which is a mathematical object that emerges from rough-path theory and provides a highly abstract and universal description of complex multimodal data streams that has recently demonstrated great success in several machine learning tasks (Kidger et al., 2019; Xie et al., 2017; Yang et al., 2022). To be more precise, we add a time dimension to $\tilde{d}$ dimensional time series $(x_t)_{t=1}^T$ and embed it into $X : [0,T] \to E := \mathbb{R}^d$ with $d = \tilde{d} + 1$. For example, this is easily done by linearly interpolating discrete time data points. We assume that X is regular (c.f. Section 3.2) and denote the space of all such regular paths by $\Omega_0([0,T],E)$. The signature of a path determines the path up to tree-like equivalence (Boedihardjo & Geng, 2015; Hambly & Lyons, 2010). Roughly speaking, there is an almost one-to-one correspondence between the signature and the path, but when restricting the path space to $\Omega_0([0,T],E)$, the signature (feature) map $S : x \mapsto S(x)$, $x \in \Omega_0([0,T],E)$, is bijective. In other words, the signature of a path in $\Omega_0([0,T],E)$ determines the path completely (Levin et al., 2016). Let $S(\Omega_0([0,T],E))$ denote the range of the signature of all the possible paths in $\Omega_0([0,T],E)$. Note that the signature map S, defined on $\Omega_0([0,T],E)$, is continuous with respect to the 1-variation topology (Lyons et al., 2007). A remarkable property of the signature is the following universal approximation property.

Theorem 2.1 Universality of signature (Levin et al., 2016). *Consider a compact set $\mathcal{K} \subset S(\Omega_0([0,T],E))$. Let $\boldsymbol{f} : \mathcal{K} \to \mathbb{R}$ be any continuous function. Then, for any $\epsilon > 0$, there exists a linear functional $\boldsymbol{L} \in T((E))^*$ acting on the signature such that*

$$\sup_{S \in \mathcal{K}} |\boldsymbol{f}(S) - \boldsymbol{L}(S)| < \epsilon. \tag{3}$$

Theorem 2.1 applies to any subspace topology on $(S(\Omega_0([0,T],E))$, which is inherited from the Hausdorff topology $T((E))$, that is finer than the weak topology. The theorem tells us that any continuous functional on the signature space can be arbitrarily well approximated by a linear combination of coordinate signatures.

Since the signature S is bijective and continuous when restricting the path space to $\Omega_0([0,T],E)$, the pushforward of the measure on the path space, $\boldsymbol{\mu}(B) := (S_{\#}\mu)(B) = \mu(S^{-1}(B))$ for B in the σ-algebra of $S(\Omega_0(J,E))$, induces the measure on the signature space. With this in mind, the W_1 on

the signature space is given by

$$W_1^{\mathrm{Sig}}(\mu,\nu) := \sup_{||\boldsymbol{f}||_{Lip,\mathcal{K}}\le 1} \mathbb{E}_{S\sim\boldsymbol{\mu}}[\boldsymbol{f}(S)] - \mathbb{E}_{S\sim\boldsymbol{\nu}}[\boldsymbol{f}(S)]\,.$$

Motivated by the universality of signature, we consider the following Sig-W_1 metric as the proxy for W_1^{Sig} by restricting the admissible test functions to be linear functionals:

$$\text{Sig-}W_1(\mu,\nu) = \sup_{||L||_{Lip}\le 1, \boldsymbol{L} \text{ is a linear functional}} \mathbb{E}_{S\sim\boldsymbol{\mu}}[\boldsymbol{L}(S)] - \mathbb{E}_{S\sim\boldsymbol{\nu}}[\boldsymbol{L}(S)]\,.$$

The Sig-W_1 metric was initially proposed in Ni et al. (2021), where the Lipschitz norm of f is obtained by endowing the underlying signature space equipped with the l^2 norm. Here, we consider a more general case, where the norm of the signature space is chosen as l^p for some $p > 1$.

In Lemma 4.5, we show that when

$$||\boldsymbol{L}||_{Lip} := \sup_{x\neq y, x,y\in \boldsymbol{T}^{p(E)}} \frac{|\boldsymbol{L}(x-y)|}{||x-y||_p}, \text{ for some } p \ge 1,$$

where $\boldsymbol{T}^p(E)$ is the set of all the tensor series elements with finite l^p norm, then Sig-W_1 admits analytic formula

$$\text{Sig-}W_1(\mu,\nu) = \|\mathbb{E}_{S\sim\boldsymbol{\mu}}[S] - \mathbb{E}_{S\sim\boldsymbol{\nu}}[S]\|_p\,.$$

The significance of this result is that Sig-W_1-GAN framework reduces the challenging min–max problem to supervised learning, without severing loss of accuracy when compared with Wasserstein distance on the path space. Figure 1 of the two-dimensional VAR(1) dataset illustrates that the SigCWGAN helps stablize the training process and accelerate the training to converge compared with the CWGAN when keeping the same conditional generator for both methods.

In the conditional setting studied here, we lift both $(X_{\mathrm{past}}, X_{\mathrm{future}})$ into the signature space, that is $(X_{\mathrm{past}}, X_{\mathrm{future}}) \mapsto (S_{\mathrm{past}}, S_{\mathrm{future}}) := (S(X_{\mathrm{past}}), S(X_{\mathrm{future}}))$. The corresponding Sig-$W_1$ distance is given

$$\begin{aligned}\text{Sig-}W_1(\mu(S_{\mathrm{past}}),\nu(S_{\mathrm{past}})) &= \|\mathbb{E}_{S\sim\boldsymbol{\mu}(S_{\mathrm{past}})}[S] - \mathbb{E}_{S\sim\boldsymbol{\nu}(S_{\mathrm{past}})}[S]\|_p \\ &= \|\mathbb{E}_{S\sim\boldsymbol{\mu}}[S_{\mathrm{future}} \mid S_{\mathrm{past}}] - \mathbb{E}_{S\sim\boldsymbol{\nu}}[S_{\mathrm{future}} \mid S_{\mathrm{past}}]\|_p..\end{aligned}$$

where S denotes $(S_{\mathrm{past}}, S_{\mathrm{future}})$. From Doob–Dynkin lemma, we know that the conditional expectations are measurable functions of S_{past}. Assuming the continuity of conditional expectation, and by the universal approximation results, these can be approximated arbitrarily well by linear functional of signature. Hence, we have

$$\mathbb{E}_{S\sim\boldsymbol{\mu}}[|S_{\mathrm{future}} - \mathbb{E}_{\boldsymbol{\mu}(S_{\mathrm{past}})}[S_{\mathrm{future}}]|^2] \approx \inf_{L \text{ linear functional}} \mathbb{E}_{S\sim\boldsymbol{\mu}}[|S_{\mathrm{future}} - L(S_{\mathrm{past}})|^2]\,. \tag{4}$$

Due to linearity of the functional L, the solution of the above optimization problem can be estimated by linear regression.

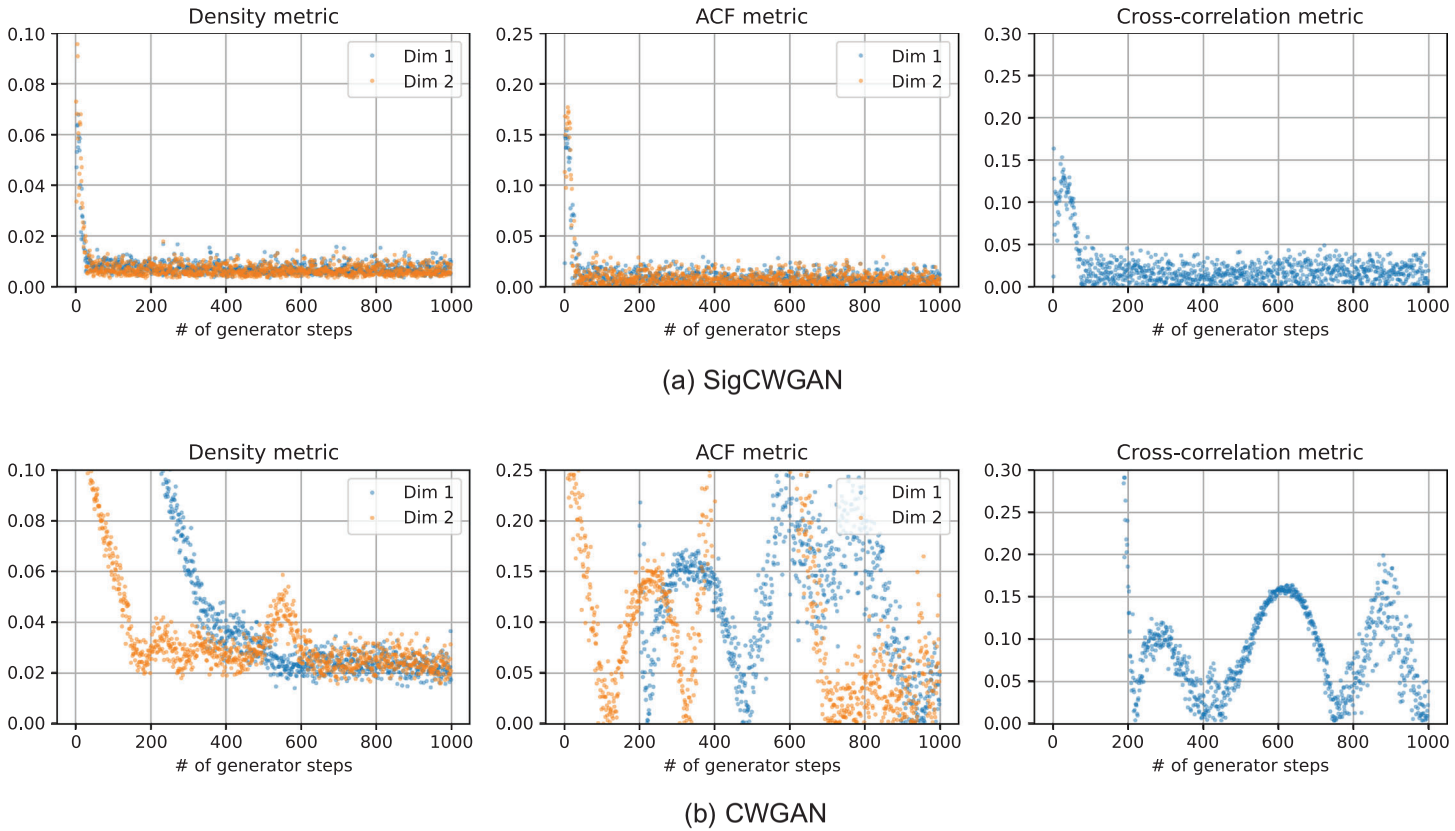

FIGURE 1 Comparison across three performance metrics (see Section 6) of training SigCWGAN with loss function (5) and CWGAN with loss function (2) for two-dimensional VAR(1), given by $X_{t+1} = \phi X_t + \epsilon_{t+1}$ with $(\epsilon_t)_{t=1}^T$ iid Gaussian-distributed random variables with co-variance matrix $\sigma\mathbf{1} + (1-\sigma)\mathbf{I}$ and autocorrelation coefficient $\phi = 0.8$ and co-variance parameter $\sigma = 0.8$. The explicit form of the model allows for an unbiased approximation of conditional expectation in (2) using Monte Carlo samples. The colors blue and orange indicate the relevant distance/score for each dimension. [Color figure can be viewed at wileyonlinelibrary.com]

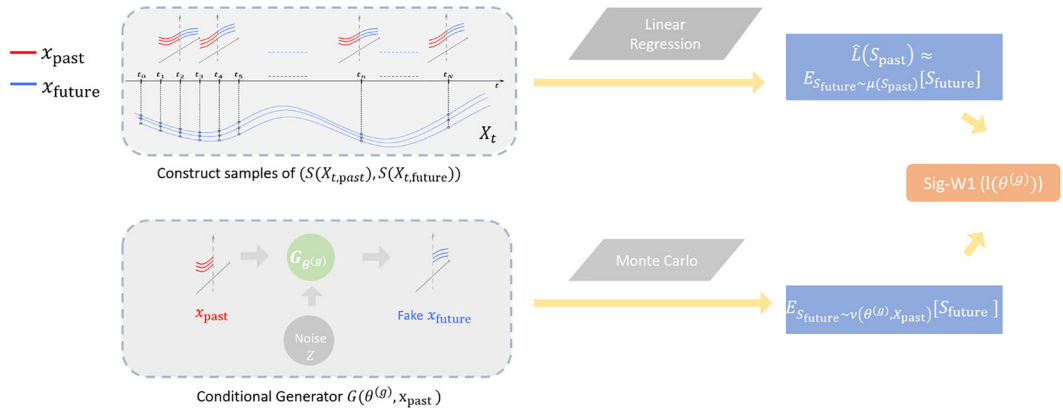

FIGURE 2 The illustration of the flowchart of SigCWGAN. [Color figure can be viewed at wileyonlinelibrary.com]

Let $\hat{\boldsymbol{L}}$ denote the linear regression estimator of the conditional expectation $x \mapsto \mathbb{E}_{S\sim\mu}[S_{\text{future}}|S_{\text{past}} = x]$.

Unlike classical W_1-GAN described above, the conditional expectation under the data measure needs to be computed only once. Complete training is then reduced to solving following supervised learning problem

$$\ell(\theta^{(g)}) := \mathbb{E}^{X_{\text{past}}}\left[||\hat{\boldsymbol{L}}(S_{\text{past}}) - \mathbb{E}_{S_{\text{future}}\sim\boldsymbol{\nu}(\theta^{(g)},X_{\text{past}})}[S_{\text{future}}]||_p\right]. \tag{5}$$

Note that for each $\theta^{(g)}$, one needs to approximate $\mathbb{E}_{S\sim\boldsymbol{\nu}(\theta^{(g)})}[S_{\text{future}}]$ using Monte Carlo simulations. A complete approximation algorithm also requires Monte Carlo approximation of outer expectation and truncation of the signature map (see Section 5.2 for exact details). The flowchart of SigCWGAN algorithm is given in Figure 2.

2.2 | Related work

In the time series domain, the unconditional generative model was approached by various works such as Koshiyama et al. (2021) and Wiese et al. (2020). Among the signature-based models, Kidger et al. (2019) used Sig-MMD, originated in Chevyrev and Oberhauser (2022), a version of the maximum mean discrepancy (MMD) with the signature feature, to generate the Ornstein–Uhlenbeck process. Independently, Ni et al. (2021) proposed the Sig-Wasserstein GAN motivated by combining the Wasssertain-1 distance and the signature feature. Also the conditional generative objective was approached by various authors. Esteban et al. (2017), Koochali et al. (2021), Fu et al. (2020), Wiese et al. (2019) used FNNs/LSTMs with recurrent conditional GANs (RCGANs), Donahue et al. (2019), Engel et al. (2019) use GANs to generating log-magnitude spectrograms and phases directly for audio synthesis, and Buehler et al. (2020) pair log-signatures with variational autoencoders (VAEs) and formulate a conditional generator in log-signature space. Conditional VAEs with the log-signature in Buehler et al. (2020) are well adapted to small data environment, but it may require an additional step of inverting synthetic log-signature to the path for time series generation. TimeGAN (Yoon et al., 2019) demonstrates the improvement by adding the

TABLE 1 Notation summary table.

Symbol	Meaning
E	$E = \mathbb{R}^d$
$T((E))$	The tensor algebra space of E
$\mathbf{T}^p(E)$	The set of all the elements in $T((E))$ with finite l^p norm
$\|\|.\|\|_p$	The l^p norm on $\mathbf{T}^p(E)$
$\|\|.\|\|_q$	The l^q norm on $T((E))^*$
X	E-valued time series of length T, that is, $X = (X_1, \dots, X_T) \in \mathbb{R}^{d\times T}$
$X_{t,\text{past}}$	The $\bar{p}$ lagged values of X_t, that is, $(X_{t-p+1}, \dots, X_t) \in \mathbb{R}^{d\times\bar{p}} =: \mathcal{X}$.
$X_{t,\text{future}}$	The next $\bar{q}$ step forecast of X_t, that is, $(X_{t+1}, \dots, X_{t+\bar{q}}) \in \mathbb{R}^{d\times\bar{q}} =: \mathcal{Y}$.
$\bar{p}$	The window size of the past path $X_{t,\text{past}}$
$\bar{q}$	The window size of the future path $X_{t,\text{future}}$
$S_{t,\text{past}}$	The signature of $X_{t,\text{past}}$
$S_{t,\text{future}}$	The signature of $X_{t,\text{future}}$

supervised loss to the adversarial loss to force network to adhere to the dynamics of the training data during sampling. The supervised loss of TimeGAN is defined in terms of the sample-wise discrepancy between the true latent variable h_{t+1} and the generated one-sample estimator $\hat{h}_{t+1}$ given h_t. However, even if the estimator $\hat{h}_{t+1}$ has the same conditional distribution as h_{t+1}, the supervised loss may not be equal to zeros, and hence it suggests that the proposed loss function might not be suitable to capture the conditional distribution of the latent variable h_{t+1} given the h_t.

Conditional moment matching network (CMMN) introduced in Ren et al. (2016) derives the conditional MMD criteria based on the kernel mean embedding of conditional distributions, which avoids the approximation issues mentioned in the above conditional WGANs. However, the performance of CMMN depends on the kernel choice and it is yet unclear how to choose the kernel on the path space. While our SigWGAN method is built on the conditional WGANs and the signature features, we would like to highlight the difference of method to the conditional WGAN and its link to CMMD. SigCWGAN resolves the computational bottleneck of the conditional WGANs given the past time series by using the analytic formula for the conditional discriminator without training. Building upon Ni et al. (2021), our work expands the SigWGAN framework from its initial application to unconditional generative models to enable conditional generative modeling. Moreover, one can view the SigCWGAN as the combination of unnormalized Sig-MMD (Chevyrev & Oberhauser, 2022) and CMMD, which has not been explored in the literature. It is worth noting that we also extend the definition of Sig-W_1 in Ni et al. (2021), from the l^2 norm of the signature space to the general l^p for some $p > 1$. We provide Table 1 to summarize the commonly used notations of our paper.

3 | SIGNATURES AND EXPECTED SIGNATURES

In order to introduce formally the optimal conditional time series discriminator, in this section, we recall basic definitions and concepts from rough path theory.

3.1 | Tensor algebra space

We start with introducing the tensor algebra space of E, where the signature of a E-valued path takes values. For simplicity, fix $E = \mathbb{R}^d$ throughout the rest of the paper. E has the canonical basis $\{e_1, \dots, e_d\}$. Consider the successive tensor powers $E^{\otimes n}$ of E.[2] If one thinks of the elements e_i as letters, then $E^{\otimes n}$ is spanned by the words of length n in the letters $\{e_1, \dots, e_d\}$, and can be identified with the space of real homogeneous noncommuting polynomials of degree n in d variables, that is, $(e_I := e_{i_1} \otimes \cdots \otimes e_{i_n})_{I=(i_1,\dots,i_n)\in\{1,\dots,d\}^n}$. We give the formal definition of the tensor algebra series as follows.

Definition 3.1. The space of all formal E-tensors series, denoted by $T((E))$ is defined to be the following space of infinite series:

$$T((E)) = \left\{ \mathbf{a} = (a_0, a_1, \dots) \middle| a_n \in E^{\otimes n}, \forall n \geq 0 \right\}.$$

It is equipped with two operations, an addition and a product defined as follows: $\forall \mathbf{a} = (a_0, a_1, \dots), \mathbf{b} = (b_0, b_1, \dots) \in T((E))$, it holds that

$$\mathbf{a} + \mathbf{b} = (a_0 + b_0, a_1 + b_1, \dots);$$

$$\mathbf{a} \otimes \mathbf{b} = (c_0, c_1, \dots).$$

where $c_n = \sum_{j=0}^{n} a_j \otimes b_{n-j}$.

We endow the space $T((E))$ with the action of $\mathbb{R}$ by $\lambda\mathbf{a} = (\lambda a_0, \lambda a_1, \dots)$ is a real noncommuntative untial algebra with the unit $\mathbf{1} = (1, 0, 0, \dots)$ Lyons et al. (2007).

Let us first introduce the function $||\cdot||_p : T((E)) \to [0, +\infty]$ for some $p \geq 1$. For any element $\mathbf{a} := \sum_{n\in\mathbb{N}} \sum_{I\in\{1,\dots,d\}^n} a_I e_I \in T((E))$,

$$||a||_p = \left(\sum_{n\in\mathbb{N}} |a_n|_p^p \right)^{1/p}, \tag{6}$$

where $|a_n|_p = (\sum_{I\in\{1,\dots,d\}^n} |a_I|^p)^{\frac{1}{p}}$.

Similarly, we define the map $||\cdot||_q : T((E))^* \to [0, +\infty]$. Define the canonical basis of the dual space $T((E))^*$, that is $(e_I^*)_{I=(i_1,\dots,i_n)\in\{1,\dots,d\}^n, n\in\mathbb{N}}$ by $\langle e_{I_1}^*, e_{I_2} \rangle = \mathbf{1}_{I_1=I_2}$. For any $L \in T((E))^*$, one can write

$$L = \sum_{n\in\mathbb{N}} \sum_{I\in\{1,\dots,d\}^n} L_I e_I^*.$$

Then $||L||_q$ is defined as

$$||L||_q = \left(\sum_{n\in\mathbb{N}} \sum_{I=(i_1,\dots,i_n)\in\{1,\dots,d\}^n} |L_I|^q \right)^{1/q}. \tag{7}$$

In particular, we consider the subspace $\mathbf{T}^p(E)$, consisting with all the elements $a \in T((E))$ with finite $||a||_p$. In this case, $||\cdot||_p$ becomes the l^p norm of $\mathbf{T}^p((E))$.

Definition 3.2. Fix some $p \geq 1$. We denote by $\mathbf{T}^p(E)$ the following space equipped with the l^p topology:

$$\mathbf{T}^p(E) := \left\{\mathbf{a} \in T((E)) \middle| \quad ||\mathbf{a}||_p < +\infty\right\}.$$

Furthermore, we define

$$\tilde{T}^p(E) = \{\mathbf{a} \in \mathbf{T}^p(E) \big| a_0 = 1\}.$$

In practice, instead of the signature (an infinite series of E-tensors), we often work with the truncated signature. Hence, we introduce the corresponding truncated tensor algebra space.

Definition 3.3. Let $n \geq 1$ be an integer. Let $B_n = \{\mathbf{a} = (a_0, a_1, ...) | a_0 = \cdots = a_n = 0\}$. The truncated tensor algebra $T^{(n)}(E)$ of order n over E is defined as the quotient algebra

$$T^{(n)}(E) = T((E))/B_n. \tag{8}$$

The canonical homomorphism $T((E)) \longrightarrow T^{(n)}(E)$ is denoted by π_n.

3.2 | Signature of time series

Embed time series in the path space

The signature feature takes a continuous function perspective on discrete time series. It allows the unified treatment on irregular time series (e.g., variable length, missing data, uneven spacing, asynchronous multidimensional data) to the path space (Chevyrev & Kormilitzin, 2016). To embed time series to the signature space, we first lift discrete time series to a continuous path of bounded 1-variation.

Let $\bar{x} = (x_t)_{t=1}^T \in \mathbb{R}^{\tilde{d} \times T}$ be a $\tilde{d}$-dimensional time series of length T. We embed $\bar{x}$ to $X : [0, T] \to \mathbb{R}^d$ with $d = \tilde{d} + 1$ as follows: (1) interpolate the cumulative sum process of $\bar{x}$ to get the d-dimensional piecewise linear path; (2) add the time dimension to the 0th coordinate of X.

Let $\Omega_0([0, T], \mathbb{R}^d)$ denote the space of continuous d-dimensional paths of finite 1-variation starting from the origin, with the 0th coordinate being the time dimension. We endow $\Omega_0([0, T], \mathbb{R}^d)$ with the 1-variation metric.[3] For any $\tilde{d}$-dimensional time series, its embedded path X lives in $\Omega_0([0, T], \mathbb{R}^d)$. Figure 3 gives one concrete example to illustrate the time series embedding.

Throughout the rest of the paper, we restrict our discussion on the path space $\Omega_0(J, E)$. However, our methodology discussed later can be applied to other methods of transforming discrete time series to the path space provided that the embedding ensures the uniqueness of the signature. The commonly used path transformations with such uniqueness property are listed in Section B.1.

The signature of the path

We first introduce the k-fold iterated integral of a path $X \in \Omega_0([0, T], \mathbb{R}^d)$. Let $I = (i_1, \dots, i_k)$ be a multi-index of length k, where $i_1, \dots, i_n \in \{0, 1, 2, \dots, d-1\}$. Let $X^{(i)}$ denote the ith coordinate of

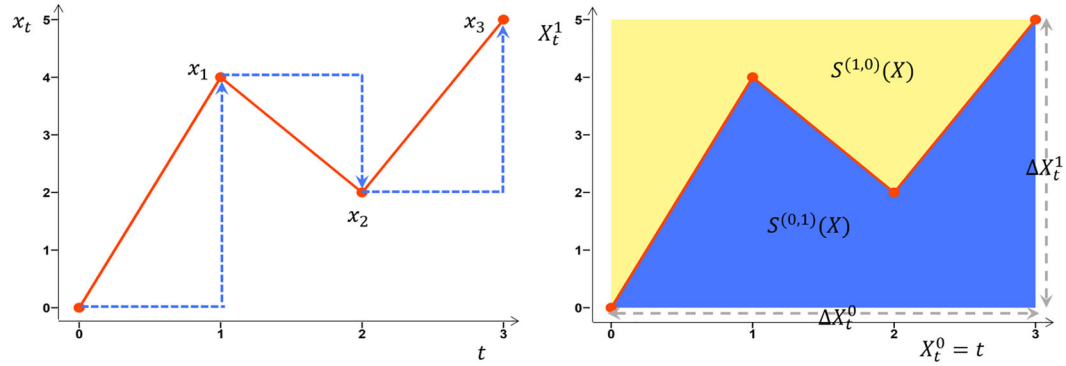

FIGURE 3 (Left) Embed one dimensional time series $\bar{x} = (x_1, x_2, x_3)$ to X (in blue) in the path space. First we compute $(X_t)_{t=0}^3$, which is the cumulative sum of $(x_t)_{t=1}^3$, that is, $X_0 = 0$ and $X_t^{(1)} = \sum_{i=1}^t x_i$, $X_t^{(0)} = t$ for $t = 1, 2, 3$. Then we linearly interpolate X to a continuous path in $\Omega_0([0, 3], \mathbb{R}^2)$; (right) embed the time series to the path space and visualize the low order signature. [Color figure can be viewed at wileyonlinelibrary.com]

X, which is a real-valued function. The iterated integral of x indexed by I is defined as

$$S^{(i_1,i_2,\ldots,i_k)}(X) = \int_{0<t_1<t_2<\cdots<t_k<T} dX_{t_1}^{(i_1)} dX_{t_2}^{(i_2)} \cdots dX_{t_k}^{(i_k)}.$$

Collecting the iterated integrals of X with all possible indices of length k gives rise to the kth fold iterated integral of X. It can also be written in the tensor form, that is,

$$\int_{0\le t_1\le t_2\le\cdots\le t} dX_{t_1} \otimes dX_{t_2} \otimes \cdots \otimes dX_{t_n} \in E^{\otimes n}.$$

Figure 3 (left) shows the one-fold iterated integral of X, which is the increment of X, that is, $X_3 - X_0$, and the two-fold iterated integral of X, which is given by

$$\mathbf{X}^{(2)} = (S^{(0,0)}(X), S^{(0,1)}(X), S^{(1,0)}(X), S^{(1,1)}(X)),$$

where $S^{(i,i)}(X) = \frac{1}{2}(\Delta X^i)^2$ and $S^{(0,1)}(X), S^{(1,0)}(X)$ are blue and yellow area in Figure 3 (right), respectively.

Now we are ready to introduce the *signature of a path* X.

Definition 3.4 (Signature of a path). Let $X \in \Omega_0(J, E)$. The signature of the path X is defined as

$$S(X) = (1, \mathbf{X}^{(1)}, \mathbf{X}^{(2)}, \ldots) \in T((E)), \tag{9}$$

where $\mathbf{X}^{(n)} = \int_{0\le t_1\le t_2\le\cdots\le t} dX_{t_1} \otimes dX_{t_2} \otimes \cdots \otimes dX_{t_n}$.

The truncated signature of the path X of degree M, denoted by $S_M(X)$ and defined by

$$S_M(X) := \pi_M(S(X)) = (1, \mathbf{X}^{(1)}, \ldots, \mathbf{X}^{(M)}).$$

Lemma 3.5. *Fix some $p \ge 1$. For any $X \in \Omega_0([0, T], \mathbb{R}^d)$, the signature of X is an element of $\mathbf{T}^p(E)$.*

Proof. It is a consequence of the factorial decay of the signature of a path of bounded 1-variation (c.f., Lemma A.2 in Appendix A). □

Lemma 3.6 (Uniqueness of signature). *For any $X \in \Omega_0([0,T],E)$, the signature of X uniquely determines X.*

Proof. We refer the proof to that of Lemma 2.14 in Levin et al. (2016). □

The *universality* and *uniqueness* of signature, described in Section 2.1, make it an excellent candidate as a feature extractor of time series.

As we mainly work on the signature space in the later section, we provide a remark on the structure of the range of S on $\Omega_0([0,T],E)$.

Remark 3.7. Let $\mathcal{K}$ denote a compact set of $\Omega_0([0,T],E)$. Then the range $S(\mathcal{K})$ is a compact set of $\mathbf{T}^p(E)$ endowed with l^p topology. We defer the proof to that of Lemma A.3 at Appendix A.

3.3 | Expected signature

Expected signature

Since the signature S is a bijective and continuous map when restricting the path space to $\Omega_0([0,T],E)$, the pushforward of the measure on the path space, $\boldsymbol{\mu}(B) := (S_{\#}\mu)(B) = \mu(S^{-1}(B))$ for B in the σ-algebra of $S(\Omega_0([0,T],E))$, induces the measure on the signature space.

Lemma 3.8. *Let μ,ν be two measures defined on the path space $\Omega_0(J,E)$. Then for $\boldsymbol{\mu}(B) := (S_{\#}\mu)(B)$ and $\boldsymbol{\nu}(B) := (S_{\#}\nu)(B)$ with B in the σ-algebra of $S(\Omega_0(J,E))$ we have*

$$\boldsymbol{\mu} = \boldsymbol{\nu} \iff \mu = \nu.$$

Proof. This is an immediate result of the bijective property of the signature map S, when S is restricted to $\Omega_0(J,E)$. □

By Proposition 6.1 in Chevyrev et al. (2016), we have the following result:

Theorem 3.9. *Let μ and ν be two measures on the path space $\Omega_0(J,E)$. Let $\boldsymbol{\mu}(B) := (S_{\#}\mu)(B)$ and $\boldsymbol{\nu}(B) := (S_{\#}\nu)(B)$ for B is in the σ-algebra of $S(\Omega_0(J,E))$. Suppose that $\mathbb{E}_{S\sim\mu}[S]$ exists and has infinite radius of convergence[4]. If $\mathbb{E}_{S\sim\mu}[S] = \mathbb{E}_{S\sim\nu}[S]$, then $\mu = \nu$.*

In other words, under the regularity condition, the distribution μ on the path space is characterized by $\mathbb{E}_{X\sim\mu}[S(X)]$. We call $\mathbb{E}_{X\sim\mu}[S(X)]$ the expected signature of the stochastic process X under measure μ. Intuitively, the signature of a path plays a role of a noncommutative polynomial on the path space. Therefore, the expected signature of a random process can be viewed as an analogy of the moment generating function of a d-dimensional random variable. For example, the expected Stratonovich signature of Brownian motion determines the law of the Brownian motion in Lyons et al. (2015). However, it is challenging to establish a general condition to guarantee the infinite radius of convergence (ROC). In fact, the study of the expected signature of stochastic processes is an active area of research. For example, the expected signature of fractional Brownian motion for the Hurst parameter $H \geq 1/2$ is shown to have the infinite ROC (Fawcett, 2002; Passeggeri, 2020),

whereas the ROC of the expected signature of stopped Brownian motion up to the first exit domain is finite (Boedihardjo et al., 2021; Li & Ni, 2022). Chevyrev et al. (2016, Theorem 6.3) provide a sufficient condition for the infinite ROC of the expected signature, potentially offering an alternative way to show the infinite ROC without directly examining the decay rate of the expected signature.

4 | SIG-WASSERSTEIN METRIC

In this section, we formalize the derivation of *Signature Wasserstein-1* (Sig-W_1) metric introduced in Section 2.1. The Sig-W_1 is a generalization of the one proposed in Ni et al. (2021) by considering the general l^p metric of the signature space.

Let $f : \Omega \to \mathbb{R}$, where Ω is a generic metric space. Define

$$||f||_{Lip,\Omega} := \sup_{x\neq y, x,y\in\Omega} \frac{|f(x)-f(y)|}{D(x,y)}, \tag{10}$$

where D is a metric defined on Ω. Let μ and ν be two compactly supported measures on the path space $\Omega_0([0,T],E)$ such that the corresponding induced measures on the signature space $\boldsymbol{\mu}$ and $\boldsymbol{\nu}$, respectively, have a compact support $\mathcal{K} \subset S(\Omega_0([0,T],E)) \subset \mathbf{T}^p(E)$. Recall that

$$W_1^{\text{Sig}}(\mu,\nu) := W_1(\boldsymbol{\mu},\boldsymbol{\nu}) = \sup_{||\boldsymbol{f}||_{Lip,\mathcal{K}}\leq 1} \mathbb{E}_{S\sim\boldsymbol{\mu}}[\boldsymbol{f}(S)] - \mathbb{E}_{S\sim\boldsymbol{\nu}}[\boldsymbol{f}(S)].$$

From the definition of the supremum, there exists a sequence of $\boldsymbol{f}_n : \mathcal{K} \to \mathbb{R}$ with bounded Lipschitz norm along which the supremum $W_1^{\text{Sig}}(\mu,\nu)$ is attained. By the universality of the signature, it implies that for any $\epsilon > 0$, for each $\boldsymbol{f}_n$, there exists a linear functional $\boldsymbol{L}_n : \mathcal{K} \to \mathbb{R}$ to approximate $\boldsymbol{f}_n$ uniformly, that is,

$$\left| \int_{\mathcal{K}} \boldsymbol{f}_n(S)\boldsymbol{\mu}(dS) - \boldsymbol{f}_n(S)\boldsymbol{\nu}(dS) - \left(\int_{\mathcal{K}} \boldsymbol{L}_n(S)\boldsymbol{\mu}(dS) - \boldsymbol{L}_n(S)\boldsymbol{\nu}(dS) \right) \right| \leq 2\epsilon.$$

As $\boldsymbol{L}_n : \mathcal{K} \to \mathbb{R}$ is linear, there is a natural extension of $\boldsymbol{L}_n$ mapping from $\mathbf{T}^p(E)$ to $\mathbb{R}$.

Motivated by the above observation, to approximate $W_1^{\text{Sig}}(\mu,\nu)$, we restrict the admissible set of $\boldsymbol{f}$ to be *linear* functionals $\boldsymbol{L} : T((E)) \to \mathbb{R}$, which leads to the following definition.

Definition 4.1 (Sig-W_1 metric). For two measures μ,ν on the path space $\Omega_0([0,T],E))$ such that their induced measures $\boldsymbol{\mu}$ and $\boldsymbol{\nu}$, respectively, has a compact support $\mathcal{K} \subset S(\Omega_0([0,T],E))$,

$$\text{Sig-}W_1(\mu,\nu) = \sup_{||\boldsymbol{L}||_{Lip}\leq 1, L \text{ is a linear functional:}} \left(\mathbb{E}_{S\sim\boldsymbol{\mu}}[\boldsymbol{L}(S)] - \mathbb{E}_{S\sim\boldsymbol{\nu}}[\boldsymbol{L}(S)]\right).$$

Here we skip the domain $\mathbf{T}^p(E)$ in the Lip norm of $||\mathbf{L}||_{Lip}$ for the simplicity of the notation.

Remark 4.2. Despite the motivation of Sig-W_1 from the approximation of W_1^{Sig}, it is hard to establish the theoretical results on the link between these two metrics. The main difficulty comes from that the uniform approximation of the continuous function f by a linear map L on $\mathcal{K}$ does not guarantee the closeness of their Lipschitz norms. We conjecture that in general, $W_1^{Sig}(\mu,\nu)$ is not

equal to Sig-$W_1(\mu,\nu)$. However, it would be interesting but technically challenging to find out the sufficient conditions such that these two metrics coincide.

To derive the analytic formulae for the Sig-W_1 metric, we shall introduce the following auxiliary lemma on the l^p norm of the tensor space $\mathbf{T}^p(E)$ and its dual space.

Lemma 4.3. *Fix $p,q>1$ such that $\frac{1}{p}+\frac{1}{q}=1$ (i.e., $q=\frac{p}{p-1}$).*
For any linear functional $\boldsymbol{L}\in\mathbf{T}^p(E)^*$, it holds that

$$\sup_{||a||_p=1}|\boldsymbol{L}a| = ||\boldsymbol{L}||_q, \tag{11}$$

Similarly, for any $a\in\mathbf{T}^p(E)$, it holds that

$$\sup_{||\boldsymbol{L}||_q\le 1}|\boldsymbol{L}a| = \sup_{||\boldsymbol{L}||_q=1}|\boldsymbol{L}a| = ||a||_p. \tag{12}$$

We refer to the proof of Lemma 4.3 in Appendix A.3.

Remark 4.4. The sequence space $L_p(\mathcal{I})$ is defined as

$$L_p(\mathcal{I}) = \left\{(a_I)_{I\in\mathcal{I}} \Big| \sum_{I\in\mathcal{I}}|a_I|^p<\infty\right\},$$

where $\mathcal{I}$ is a general index set and $p\ge 1$. It is well known that the dual space of $L_p(\mathcal{I})$ for $p\ge 1$ has naturally isomorphic to $L_q(\mathcal{I})$. This isomorphism is exactly the same as the map $L^*:\mathbf{T}^p(E)\setminus\{0\}\to\mathbf{T}^p(E)^*\setminus\{0\}: a\to L^*(a)$ used in our proof. Similarly, the dual space of $L_p(\mathcal{I})^*$ has a natural isomorphism with $L_p(\mathcal{I})$ for any $p>1$.

By exploiting the linearity of the functional $\boldsymbol{L}\in\mathbf{T}^p(E)^*$, we can compute the Lip norm of L analytically for D being the l^p norm of $\mathbf{T}^p(E)$ without the need of numerical optimization. By Lemma 4.3, the Lip norm of $\boldsymbol{L}$ is the L_p norm of $\boldsymbol{L}$, given as

$$||\boldsymbol{L}||_{Lip} := \sup_{x\neq y,x,y\in\mathbf{T}^p(E)}\frac{|\boldsymbol{L}(x-y)|}{||x-y||_p} = \sup_{||a||_p=1}|\boldsymbol{L}a| = ||\boldsymbol{L}||_q,$$

where $\frac{1}{p}+\frac{1}{q}=1$ and $D(x,y)=||x-y||_p$ with some $p>1$.
The simplification of the Lip norm enables us to derive an analytic formula of the corresponding Sig-W_1 metric.

Lemma 4.5. *For two measures μ,ν on the path space $\Omega_0([0,T],E)$ such that their induced measures $\boldsymbol{\mu}$ and $\boldsymbol{\nu}$ have a compact support $\mathcal{K}\subset S(\Omega_0([0,T],E))$. Then it holds that*

$$\textit{Sig-}W_1(\mu,\nu) = \|\mathbb{E}_{S\sim\boldsymbol{\mu}}[S]-\mathbb{E}_{S\sim\boldsymbol{\nu}}[S]\|_p = \|\mathbb{E}_{X\sim\mu}[S(X)]-\mathbb{E}_{X\sim\nu}[S(X)]\|_p. \tag{13}$$

Proof. Let a linear functional $\boldsymbol{L} : \mathcal{K} \to \mathbb{R}$ endowed with the Lip norm when $D(x, y) = ||x - y||_p$. In this case, the Lip norm coincides with l^q norm. The compact support $\mathcal{K}$ of $\boldsymbol{\mu}$ and $\boldsymbol{\nu}$ ensures that $\mathbb{E}_{S\sim\boldsymbol{\mu}}(S)$ and $\mathbb{E}_{S\sim\boldsymbol{\mu}}(S)$ are in $\mathbf{T}^p(E)$. Let $a := \mathbb{E}_{S\sim\boldsymbol{\mu}}(S) - \mathbb{E}_{S\sim\boldsymbol{\nu}}(X))$ and $a = (a_I)_I$. Then by Lemma 4.3, one can derive the analytic formula of Sig-W_1 metric as follows:

$$\text{Sig-}W_1(\mu, \nu) = \sup_{||\boldsymbol{L}||_q \le 1} \boldsymbol{L}(\mathbb{E}_{S\sim\boldsymbol{\mu}}(S)) - \boldsymbol{L}(\mathbb{E}_{S\sim\boldsymbol{\nu}}(S)) = \sup_{||\boldsymbol{L}||_q \le 1} \boldsymbol{L}(a) = ||a||_p.$$

□

Remark 4.6. When $p = 2$, Sig-W_1 is the same as the unnormalised Sig-MMD metric proposed in Chevyrev and Oberhauser (2022). The theoretical results in Chevyrev and Oberhauser (2022) might be useful for studying the properties of Sig-Wasserstein metric.

Throughout the rest of the paper, by default, we use Sig-W_1 metric when D is l^2 norm on $T((E))$, that is, $\text{Sig-}W_1(\mu, \nu) = \|\mathbb{E}_{X\sim\mu}[S(X)] - \mathbb{E}_{X\sim\nu}[S(X)]\|_2$. In practice, we truncate the Sig-$W_1(\mu, \nu)$ up to degree M, that is,

$$\text{Sig-}W_1^M(\mu, \nu) = \|\mathbb{E}_{X\sim\mu}[S_M(X)] - \mathbb{E}_{X\sim\nu}[S_M(X)]\|_2.$$

5 | SIG-WASSERSTEIN GANS FOR CONDITIONAL LAW

In this section, we introduce a general framework, so-called conditional Sig-Wasserstein GAN (SigCWGAN) based on Sig-W_1 metric to learn the conditional distribution $\mu(X_{\text{future}}|X_{\text{past}})$ from data x. The C-SigWGAN algorithm is mainly composed of two steps:

1. We apply a one-off linear regression to learn the conditional expected signature under true measure $\mathbb{E}_{X_{\text{future}}\sim\mu(X_{\text{past}})}[S(X_{\text{future}})]$ (see Section 5.1);
2. We solve an optimization problem to find optimal parameters $\theta^{(g)}$ of the conditional generator, when using loss (5) (see Section 5.2).

In the last subsection of this section, we propose a conditional generator, that is, AR-FNN generator, which is a nonlinear generalization of the classical autoregressive models by using a feed-forward neural network. It can generate the future time series of arbitrary length.

5.1 | Learning the conditional expected signature under the true measure

The problem of estimating the conditional expected signature under the true measure $\boldsymbol{\mu}(S_{\text{past}})$, by Equation (4) and the universality of the signature (Theorem 2.1), can be viewed as a linear regression task, with the signature of the past path and future path respectively (Levin et al., 2016).

More specifically, given a long realization of $x := (x_1, \dots, x_T) \in \mathbb{R}^{d\times T}$ and fixed window size of the past and future path $\bar{p}, \bar{q} > 0$, we construct the samples of past/future path pairs $(X_{\text{past}}, X_{\text{future}})$

in a rolling window fashion, where the ith sample is given by

$$\left(x_{\text{past}}^{(i)}, x_{\text{future}}^{(i)}\right) = \left(x_{\text{past},i+\bar{p}-1}, x_{\text{future},i+\bar{q}-1}\right).$$

Assuming stationarity of the time series, the samples of past and future signature pairs are identically distributed

$$\left(S_{M_1}\left(x_{\text{past}}^{(i)}\right), S_{M_2}\left(x_{\text{future}}^{(i)}\right)\right)_i \overset{d}{\sim} \left(S_{M_1}\left(X_{\text{past}}\right), S_{M_2}(X_{\text{future}})\right),$$

where M_1, M_2 are the degrees of the signature of the past and future paths, which can be chosen by cross-validation in terms of fitting result. One may refer to Fermanian (2022) for further discussion on the choice of the degree of the signature truncation.

In principle, linear regression methods on the signature space could be applied to solve this problem using the above constructed data. When we further assume that under the true measure,

$$S_{M_2}\left(X_{\text{future}}^{(i)}\right) = L\left(S_{M_1}\left(X_{\text{past}}^{(i)}\right)\right) + \epsilon_i,$$

where $\epsilon_i \overset{iid}{\sim} \epsilon$ and $\mathbb{E}[\epsilon_i | X^{(i)}] = 0$, then an ordinary least squares regression (OLS) can be directly used. This simple linear regression model on the signature space achieves satisfactory results on the numerical examples of this paper. But it could be potentially replaced by other sophisticated regression models when dealing with other datasets.

We highlight that this supervised learning module to learn $\mathbb{E}_{\mu(X_{\text{past}})}[S_M(X_{\text{future}})]$ is one-off and can be done prior to the generative learning. It is in striking contrast to the conditional WGAN learning, which requires to learn $\mathbb{E}_{\mu(X_{\text{past}})}[f_\alpha(X_{\text{future}})]$ every time the discriminator f_α is updated, and hence saves significant computational cost.

5.2 | Sig-Wasserstein GAN algorithm for conditional law

We recall that in order to quantify the goodness of the conditional generator $\nu(\theta^{(g)}, x_{\text{past},t}) := G(\theta^{(g)}, x_{\text{past}})_{\#}\mu_z$, we defined the loss

$$\ell(\theta^{(g)}) := \mathbb{E}^{X_{\text{past}}}\left[\left|\left|\hat{\boldsymbol{L}}(S_{\text{past}}) - \mathbb{E}_{S_{\text{future}}\sim\boldsymbol{\nu}(\theta^{(g)}, X_{\text{past}})}[S_{\text{future}}]\right|\right|_p\right],$$

where $\hat{\boldsymbol{L}}$ denotes the linear regression estimator for the conditional expectation $\hat{\boldsymbol{L}} : x \mapsto \mathbb{E}_{S\sim\boldsymbol{\mu}}[S_{\text{future}} | S_{\text{past}} = x]$. Given the conditional generator $G(\theta^{(g)}, \cdot)$, the conditional expected signature $\mathbb{E}_{X\sim\nu(X_{\text{past}},\theta^{(g)})}[S(X)]$ can be estimated by Monte Carlo method. We denote by $\hat{\nu}_i$ the empirical approximation of $\nu(\theta, x_{\text{past}}^{(i)})$, computed by sampling the future trajectory $\hat{X}_{t+1:t+\bar{q}}^{(t)}$ using $G(\theta^{(g)}, \cdot)$ and a conditioning variable $x_{\text{past},t}$. This leads to the following empirical loss function:

$$\ell^{(N)}\left(\theta^{(g)}\right) := \frac{1}{N}\sum_{i=1}^{N}\left|\left|\hat{L}_\mu\left(S_{M_1}(x_{\text{past}}^{(i)})\right)\right) - \mathbb{E}_{\hat{\nu}_i}\left[S_{M_2}\left(x_{\text{future}}^{(i)}\right)\right]\right|\right|_p. \tag{14}$$

ALGORITHM 1 Pseudocode of SigCWGAN

Input: $(x_t)_{t=1}^T$, the signature degree of future path M_2, the signature degree of past path M_1, the length of future path $\bar{q}$, the length of past path $\bar{p}$, learning rate η, batch size B, the number of epochs N, number of Monte Carlo samples N_{MC}.

Output: θ—the optimal parameter of the generator $G(\theta, \cdot)$.

Compute truncated signature of the past and future paths: $(S_{M_1}(x_{t-\bar{p}+1:t}), S_{M_2}(x_{t+1:t+\bar{q}}))_t$.
Compute linear regression coefficient $\hat{L}$ using $(S_{M_1}(x_{t-\bar{p}+1:t}), S_{M_2}(x_{t+1:t+\bar{q}}))_t$. (See Section 5.1.)
Initialize the parameters θ of the generator.
for $i = 1 : N$ **do**
  ▷ Denote the set of time index of the batch as $\mathcal{T}_B$.
  for $j = 1 :$ # of batches **do**
    We randomly select the set of time index of batch size B, denoted by $\mathcal{T}$.
    Initialize $l^{(B)}(\theta) \leftarrow 0$.
    for $t \in \mathcal{T}_B$ **do**
      Simulate n_{MC} samples of the simulated future path segments $(\hat{x}^{(j)})_{j=1}^{n_{\mathrm{MC}}}$ by the generator $G(\theta, \cdot)$ given the past path $x_{t-\bar{p}+1:t}$.
      Compute

$$\hat{\mathbb{E}}_{X\sim\nu(\theta,x_{t-\bar{p}+1:t})}[S_{M_2}(X)] \leftarrow \frac{1}{n_{\mathrm{MC}}}\sum_{j=1}^{n_{\mathrm{MC}}} S_{M_2}(\hat{x}^{(j)}).$$

      Update $l^{(B)}(\theta) \leftarrow l^{(B)}(\theta) + \|\hat{L}(S_{M_1}(x_{t-\bar{p}+1:t})) - \hat{\mathbb{E}}_{X\sim\nu(\theta,x_{t-\bar{p}+1:t})}[S_{M_2}(X)]\|_2$.
  $\theta \leftarrow \theta - \eta\frac{dl^{(B)}(\theta)}{d\theta}$.
return θ.

Using empirical loss function (14), one updates the generator parameters $\theta^{(g)}$ with stochastic gradient descent algorithm until it converges or achieves the maximum number of epochs. See Algorithm 1 for pseudocode.

5.3 | The conditional AR-FNN generator

In this subsection, we further assume that the target time series X is stationary and satisfies the following autoregressive structure, that is,

$$X_{t+1} = g(X_{t,\mathrm{past}}, \varepsilon_{t+1}), \tag{15}$$

where $f : \mathcal{X} \times \mathcal{Z} \to \mathbb{R}^d$ is continuous and $(\varepsilon_t)_t$ are i.i.d. random variables and ϵ_t and $X_{t,\mathrm{past}}$ are independent. Time series of such kind include the autoregressive model (AR) and the Autoregressive conditional heteroskedasticity (ARCH) model.

The proposed conditional AR-FNN generator is designed to capture the autoregressive structure of the target time series by using the past path $X_{\mathrm{past},t}$ as additional input for the AR-FNN generator. The function f in Equation (15) is represented by forward neural network with residual connections (He et al., 2016) and parametric ReLUs as activation functions (He et al., 2015) (see Section B.2 for a detailed description).

We first consider a step-1 conditional generator $G_1(\theta^{(g)}, \cdot) : \mathbb{R}^{d\times\bar{p}} \times \mathcal{Z} \to \mathbb{R}^d$, which takes the past path x and the noise vector Z_1 to generate a random variable to mimic the conditional distribution of step-1 forecast $\mu(X_{t+1}|X_{\text{past},t} = x)$. Here the noise vector Z_1 has the standard normal distribution in $\mathcal{Z} = \mathbb{R}^{d_Z}$.

One can generate the future time series of arbitrary length $\bar{q} \geq 1$ given x_{past} by applying $G_1(\theta^{(g)}, \cdot)$ in a rolling window fashion with i.i.d. noise vector $(Z_t)_t$ as follows. Given $x_{\text{past}} = (\mathrm{x}_1, \dots, \mathrm{x}_{\bar{p}}) \in \mathbb{R}^{d\times\bar{p}}$, we define time series $(\hat{x}_t)_t$ inductively; we first initialize the first $\bar{p}$ term $\hat{x}$ as x_{past}, and then for $t > \bar{p}$, use $G_1(\theta^{(g)}, \cdot)$ with the $\bar{p}$-lagged value of $\hat{x}_t$ conditioning variable and the noise Z_t to generate $\hat{x}_{t+1}$; in formula,

$$\hat{x}_t = \begin{cases} \mathrm{x}_t, & \text{if } t \leq \bar{p}; \\ G_1(\theta^{(g)}, \underbrace{\hat{x}_{t-\bar{p}}, \dots, \hat{x}_{t-1}}_{\bar{p} \text{ lagged values of } \hat{x}_t}, Z_t), & \text{if } t > \bar{p}. \end{cases} \tag{16}$$

Therefore, we obtain the step-$\bar{q}$ conditional generator, denoted by $G_q(\theta^{(g)}, \cdot) : \mathbb{R}^{d\times\bar{p}} \to \mathbb{R}^{d\times\bar{q}}$ and defined by $x_{\text{past}} \mapsto (\hat{x}_{\bar{p}+1}, \dots, \hat{x}_{\bar{p}+\bar{q}})$, where $(\hat{x}_{\bar{p}+1}, \dots, \hat{x}_{\bar{p}+\bar{q}})$ is defined in Equation (16). We omit $\bar{q}$ in $G_{\bar{q}}$ for simplicity. (See Algorithm 2 in Supplementary Material.)

6 | NUMERICAL EXPERIMENTS

To benchmark with SigCWGAN, we consider the baseline conditional WGAN (CWGAN) to compare the performance and training time. Besides, we benchmark SigCWGAN with three representative generative models for the time-series generation, that is, (1) TimeGAN Yoon et al. (2019), (2) RCGAN (Hyland et al., 2018)—a conditional GAN and (3) GMMN (Li et al., 2015)—an unconditional MMD with Gaussian kernel. For a fair comparison, we use the same neural network generator architecture, namely the three-layer AR-FNN described in Section B.2, for all the above generative models. Furthermore, we compare the proposed SigCWGAN with Generalized autoregressive conditional heteroskedasticity model (GARCH), which is a popular econometric time series model.

To demonstrate the model's ability to generate realistic multidimensional time series in a controlled environment, we consider synthetic data generated by the Vector Autoregressive (VAR) model, which is a key illustrative example in TimeGAN (Yoon et al., 2019). We also provide two financial datasets, that is, the SPX/DJI index data and Bitcoin-USD data to validate the efficacy of the proposed SigCWGAN model on empirical applications. The additional example of synthetic data generated by ARCH model is provided in the appendix.

To assess the goodness of the fitting of a generative model, we consider three main criteria (a) the marginal distribution of time series; (b) the temporal and feature dependence; (c) the usefulness (Yoon et al., 2019)—synthetic data should be as useful as the real data when used for the same predictive purposes (i.e., train-on-synthetic, test-on-real).[5] In the following, we give the precise definition of the test metrics. More specially, we use $\mathcal{D}_{\text{real}} := (x^{(i)}_{\text{future}})_{i=1}^N$ and $\mathcal{D}_{\text{fake}} := (\hat{x}^{(i)}_{\text{future}})_{i=1}^N$ to compute the test metrics, where $\hat{x}^{(i)}_{\text{future}}$ is a simulated future trajectory sampling by the conditional generator $G(\theta^{(g)}, x^{(i)}_{\text{past}})$. $\mathcal{D}_{\text{real}}$ and $\mathcal{D}_{\text{fake}}$ are the samples of the $\mathbb{R}^{d\times\bar{q}}$-valued random variable X_{future} under real measure and synthetic measure resp. The test metrics are defined below.

- **Metric on marginal distribution**: For each feature dimension $i \in \{1, \dots, d\}$, we compute two empirical density functions (epdfs) based on the histograms of the real data and synthetic data resp. denoted by $\hat{df}_r^i$ and $\hat{df}_G^i$. We take the absolute difference of those two epdfs as the metric on marginal distribution averaged over feature dimension, that is,

$$\frac{1}{d}\sum_{i=1}^{d} |\hat{df}_r^i - \hat{df}_G^i|_1.$$

- **Metric on dependency**:

  (1) Temporal dependency: We use the absolute error of the auto-correlation estimator by real data and synthetic data as the metric to assess the temporal dependency. For each feature dimension $i \in \{1, \dots, d\}$, we compute the auto-covariance of the ith coordinate of time series data X with lag value k under the real measure and the synthetic measure, respectively, denoted by $\rho_r^i(k)$ and $\rho_G^i(k)$. Then the estimator of the lag-1 auto-correlation of the real/synthetic data is given by $\frac{\rho_r^i(1)}{\rho_r^i(0)}/\frac{\rho_G^i(1)}{\rho_G^i(0)}$. The ACF score is defined to be the absolute difference of lag-1 auto-correlation given as follows:

$$\frac{1}{d}\sum_{i=1}^{d}\left|\frac{\rho_r^i(1)}{\rho_r^i(0)} - \frac{\rho_G^i(1)}{\rho_G^i(0)}\right|.$$

  Note $\rho_r^i(k)$ and $\rho_r^i(k)$ can be estimated empirically by Equations (C.1) and (C.2) in Appendix C, respectively, which allows us to compute the ACF score on the dataset. In addition, we present the ACF plot, which illustrates the autocorrelation of each coordinate of the time series with different lag values. The synthetic data's quality is evaluated by how closely its ACF plot resembles that of the real data, as it indicates the synthetic data's ability to capture long-term temporal dependencies.

  (2) Feature dependency: For $d > 1$, we use the l^1 norm of the difference between cross correlation matrices. Let $\tau_r^{i,j}$ and $\tau_G^{i,j}$ denote the correlation of the ith and jth feature of time series under real measure and synthetic measure, respectively. The metric on the correlation between the real data and synthetic data is given by l^1 norm of the difference of two correlation matrices, that is,

$$\sum_{i=1}^{d}\sum_{j=1}^{d}\left|\tau_r^{i,j} - \tau_G^{i,j}\right|.$$

  We defer the estimation of the correlation matrix $\tau_r^{i,j}$ and $\tau_G^{i,j}$ from the true data and fake data to Appendix C.

- R^2 **comparison**: Following Esteban et al. (2017) and Yoon et al. (2019), we consider the problem of predicting next-step temporal vectors using the lagged values of time series using the real data and synthetic data. First, we train a supervised learning model on real data and evaluate it in terms of R^2(TRTR). Then we train the same supervised learning model on synthetic data and evaluate it on the real data in terms of R^2 (TSTR). The closer two R^2 are, the better the generative model it is. To assess the performance of the proposed SigCWGAN to generate the longer time series, we consider the R^2 score for the regression task to predict the next q-step, where q can be even larger than $\bar{q}$.

TABLE 2 Numerical results of VAR(1) for $d = 3$ with fixed training time of 2 min.

Metrics	Marginal distribution	Auto-correlation	R^2(%)	Sig-W_1
SigCWGAN	0.0314	**0.0085**	**0.0394**	**0.4286**
CWGAN	0.0086	0.0110	0.0350	0.4384
TimeGAN	0.0243	0.0320	0.0229	0.4680
RCGAN	0.0095	0.0332	0.0214	0.4466
GMMN	**0.0084**	0.0298	0.0026	0.4499

The train and test split is 80 and 20%, respectively, in all the numerical examples. We conduct the hyper-parameter tuning for the signature truncation level. We set $p = 2$ in the l^p norm used in the Sig-W_1 metric. Appendix B contains the additional information on implementation details of SigCWGAN, including path transformations and network architecture of the generator. We refer the Appendix C for more details on the evaluation metrics. We also provide the extensive supplementary numerical results of VAR(1) data, ARCH(1) data and empirical data in Appendix D. Implementation of SigCWGAN can be found in https://github.com/SigCGANs/Conditional-Sig-Wasserstein-GANs.

6.1 | Synthetic data generated by vector autoregressive model

In the d-dimensional VAR(1) model, time series $(X_t)_{t=1}^T$ are defined recursively for $t \in \{1, \dots, T-1\}$ through

$$X_{t+1} = \phi X_t + \epsilon_{t+1}, \tag{17}$$

where $(\epsilon_t)_{t=1}^T$ are iid Gaussian-distributed random variables with co-variance matrix $\sigma\mathbf{1} + (1-\sigma)\mathbf{I}$; $\mathbf{I}$ is a $d \times d$ identity matrix. Here, the coefficient $\phi \in [-1, 1]$ controls the auto-correlation of the time series and $\sigma \in [0, 1]$ the correlation of the d features. In our benchmark, we investigate the dimensions $d = 1, 2, 3$ and various (σ, ϕ). We set $T = 40,000$ and $\bar{p} = \bar{q} = 3$. In this example, the optimal degree of signature of both past paths and future paths is 2.

First, we empirically prove that the proposed SigCWGAN can serve as an enhancement of CGWAN model. One can see from Figure 4, when the CWGAN training is fed into a more reliable estimator of the conditional mean under real measure $\mathbb{E}_{\mu(x_{\text{past}})}[f(X_{\text{future}})]$, the training tends to converge faster. However, the commonly used one-sample estimator (x_{future}) in the CWGAN training may suffer from large variance, leading to inefficiency of training. In contrast to it, the SigCWGAN may alleviate this problem by its supervised learning module. Additionally, the simplification of the min–max game to optimization via SigCWGAN leads to further acceleration and stablization of training SigCWGANs, and hence brings the performance boost, as shown in Table 2. Figure 4 illustrates that the SigCWGAN has a better fitting than CWGAN in terms of conditional law as the estimated mean (and standard deviation) is closer to that of the true model compared with CWGAN. Moreover, Tables D.1–D.3 show that the SigCWGAN consistently beats the CWGAN in terms of performance for varying d, ϕ, and σ.

We then proceed with the comparison of CSigWGN with the other state-of-the-art baseline models. Across all dimensions, we observe that the CSigWGAN has a comparable performance or outperforms the baseline models in terms of the metrics defined above. In particular, we find that

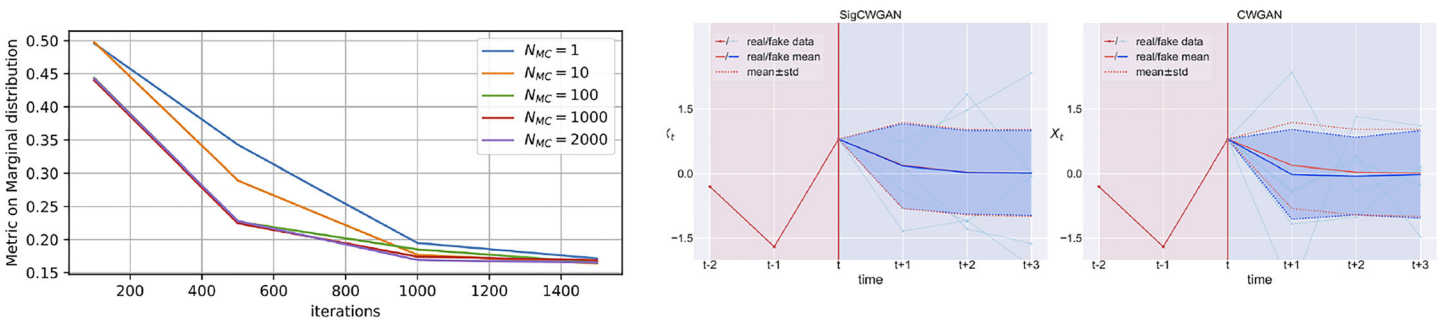

FIGURE 4 (Left) Comparison of the performance on CWGAN in terms of metric on the marginal distribution for varying N_{MC}. This experiment is conducted on a three-dimensional VAR(1) dataset generated by Equation (17) with $\phi = \sigma = 0.8$. We use the Monte-Carlo estimator of the conditional mean $(\mathbb{E}_{\mu(x_{\mathrm{past}})}[f(\theta^{(d)})(X_{\mathrm{future}})])$ generated by the ground truth model for the CWGAN training. The larger number N_{MC} of Monte Carlo approximation, the better conditional mean under the true measure. (Right) Comparison of the performance of SigCWGAN and CWGAN in terms of fitting the conditional distribution of future time series given one past path sample on one-dimensional VAR(1) dataset. [Color figure can be viewed at wileyonlinelibrary.com]

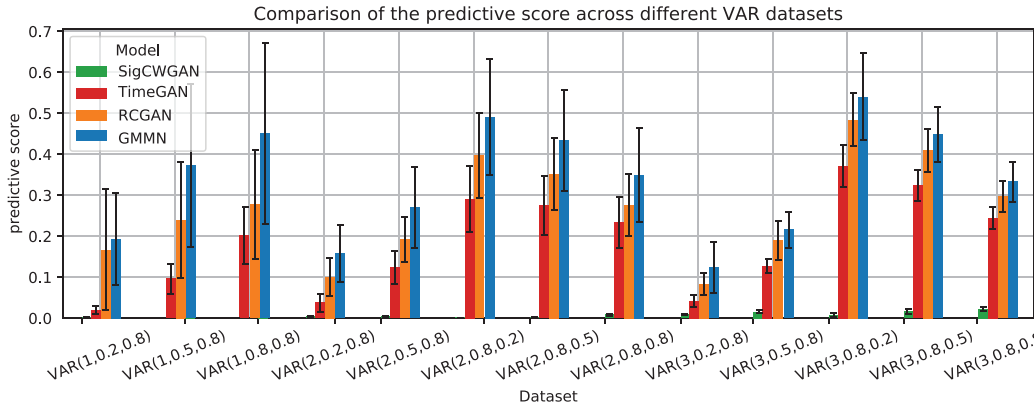

FIGURE 5 Comparison of predictive score across the VAR(1) datasets. The three numbers in the bracket indicate the hyperparameters d, ϕ, σ used to generate the corresponding VAR dataset. The predictive score was computed by taking the absolute difference of the R^2 obtained from TSTR and TRTR. [Color figure can be viewed at wileyonlinelibrary.com]

as the dimension increases, the performance of SigCWGANs exceeds baselines. We illustrate this finding in Figure 5, which shows the relative error of TSTR R^2 when varying the dimensionality of VAR(1). Observe that the SigCWGAN remains a very low relative error, but the performance of the other models deteriorates significantly, especially the GMMN.

Moreover, we validate the training stability of different methods. Figure 6 shows the development of the loss function and ACF scores through the course of training for the three-dimensional VAR(1) model. It indicates the stability of the SigCWGAN optimization in terms of training iterations, in contrast to all the other algorithms, especially RCGAN and TimeGAN that involve a min–max optimization, as identified in the 1st challenge in Section 2. While the ACF scores of the baseline models oscillate heavily, the SigCWGAN ACF score and Sig-W_1 distance converge nicely towards zero. Also, although the MMD loss converges nicely towards zero, in contrast, the ACF scores do not converge. This highlights the stability and usefulness of the Sig-W_1 distance as a loss function.

To assess the efficiency of different algorithms, we train all the algorithms for the same amount of time (2 min) and compare the test metrics of each method. Table 2 shows a higher efficiency of SigCWGAN, which yields the best performance in terms of all the metrics except for the metric on the marginal distribution.

Furthermore, the SigCWGAN has the advantage of generating the realistic long time series over the other models, which is reflected by that the marginal density function of a synthetic sampled path of 80,000 steps is much closer to that of real data than baselines in Figure 7.

6.2 | SPX and DJI index dataset

The dataset of the S&P 500 index (SPX) and Dow Jones index (DJI) consists time series of indices and their realized volatility, which is retrieved from the Oxford-Man Institute's "realized library" (Heber et al., 2009). We aim to generate a time series of both the log return of the close prices and the log of median realized volatility of (a) the SPX only; (b) the SPX and DJI. Here we choose the length of past and future path to be 3. By cross-validation, the optimal degree of signature ($M_1 = M_2$) is 3 and 2 for the SPX dataset and SPX/DJI dataset, respectively.

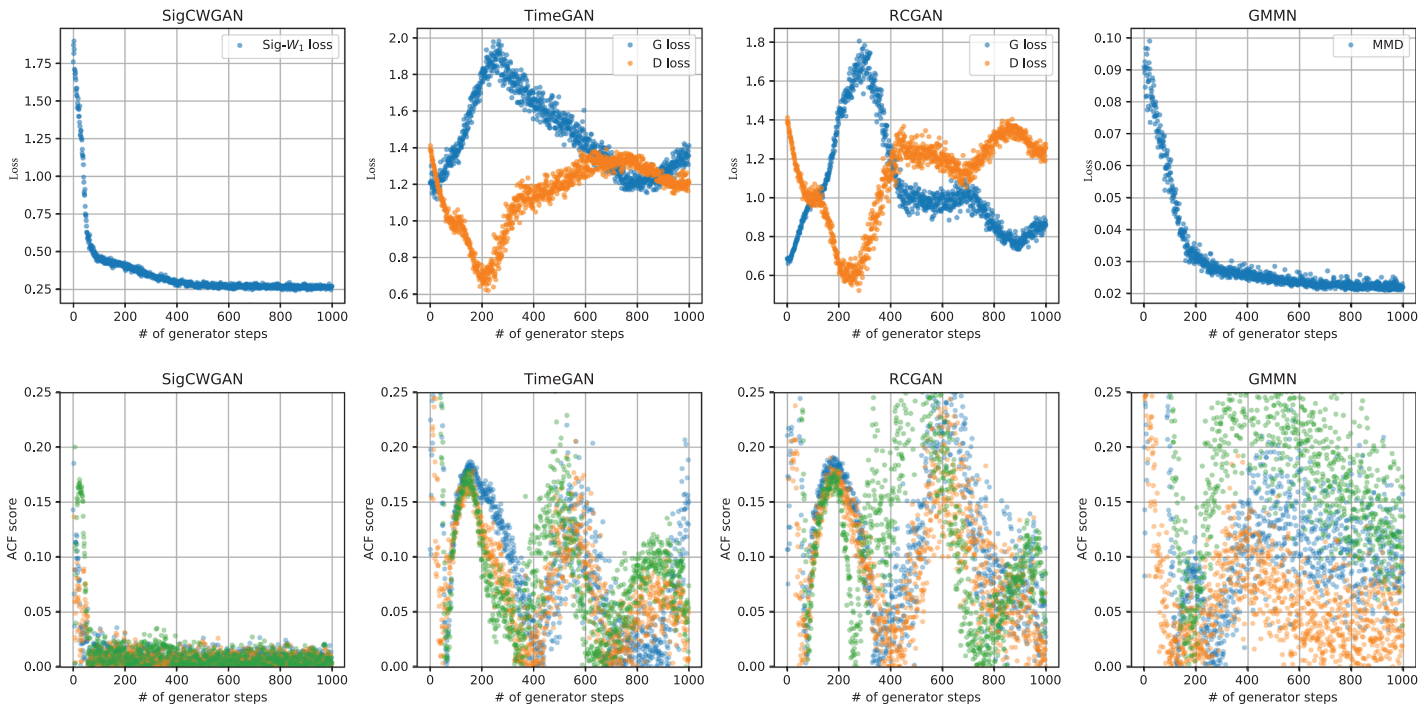

FIGURE 6 (Upper panel) Evolution of the training loss functions. (Lower panel) Evolution of the ACF scores. Each color represents the ACF score of each feature dimension. Results are for the 3-dimensional VAR(1) model based on Eqn. (17) for $\phi = 0.8$ and $\sigma = 0.8$. [Color figure can be viewed at wileyonlinelibrary.com]

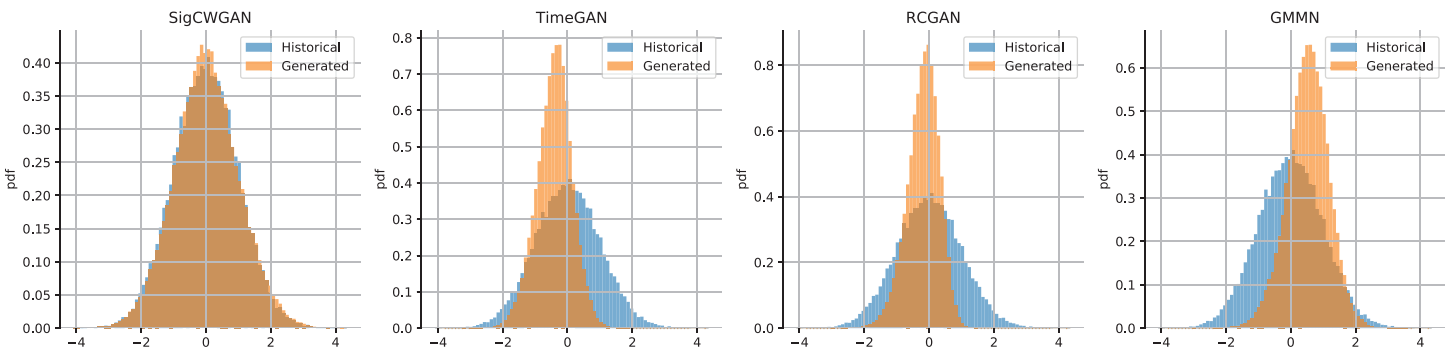

FIGURE 7 Comparison of the marginal distributions of one long sampled path (80,000 steps) with the real distribution. [Color figure can be viewed at wileyonlinelibrary.com]

TABLE 3 Numerical results of the stock datasets. In each cell, the left/right number are the result for the SPX data/the SPX and DJI data, respectively. We use the relative error of TSTR R^2 against TRTR R^2 as the R^2 metric.

Metrics	Marginal distribution	Auto-correlation	Correlation	R^2(%)	Sig-W_1
SigCWGAN	0.01730, 0.01674	0.01342, **0.01192**	**0.01079**, **0.07435**	2.996, 7.948	**0.18448**, **4.36744**
TimeGAN	0.02155, 0.02127	0.05792, 0.03035	0.12363, 0.61488	5.955, 8.586	0.58541, 5.99482
RCGAN	0.02094, **0.01655**	0.03362, 0.04075	0.04606, 0.15353	**2.788**, **7.190**	0.47107, 5.43254
GMMN	0.01608, 0.02387	**0,01283**, 0.02676	0.04651, 0.22380	9.049, 7.384	0.59073, 6.23777
GARCH	**0.01583**,0.01670	0.13392, 0.11337	0.15791, 0.7290	12.1253, 12.5686	0.64825, 6.15344

TABLE 4 Numerical results of BTC-USD data experiment. We use the relative error of TSTR R^2 against TRTR R^2 as the R^2 metric.

Metrics	Marginal distribution	Auto-correlation	R^2(%)	Sig-W_1
SigCWGAN	**2.0532**	0.091	0.3320	**0.0829**
TimeGAN	2.8037	0.1203	0.7582	0.1675
RCGAN	2.8603	**0.0532**	**0.3165**	0.0994
GMMN	2.8212	0.2093	0.3904	0.0846
GARCH	4.5063	0.0872	123.77	2.73

Table 3 shows that SigCWGAN achieves the superior or comparable performance to the other baselines. The SigCWGAN generates the realistic synthetic data of the SPX and DJI data shown by the marginal distribution comparison with that of real data in Figure 8. For the SPX only data, GMMN performs slightly better than our model in terms of the fitting of lag-1 auto-correlation and marginal distribution ($\leq$0.0013), but it suffers from the poor predictive performance and feature correlation in Table 3 and Figure 9. When the SigCWGAN is outperformed, the difference is negligible. Furthermore, the test metrics, that is, the ACF loss and density metric, of our model are evolving much smoother than the test metrics of the other baseline models shown in Figure D.7. Moreover, the ACF plot shown in Figure 10 shows that SigCWGAN has the better fitting for the auto-correlation for various lag values, which indicates the superior performance in terms of capturing long temporal dependency.

It is worth noting that our SigCWGAN model outperforms GARCH, the classical and widely used time series model in econometrics, on both the SPX and SPX/DJI data, as shown in Table 3. The poor performance of the GARCH model could be attributed to its parametric nature and the potential issues of model mis-specification when applied to empirical data.

6.3 | Bitcoin-USD dataset

The Bitcoin-USD dataset contains hourly data of Bitcoin price in USD from 2021 to 2022. We use the data in 2021 (2022) for the training (testing), respectively, which are illustrated in Figure 11. We apply our method to learn the future log-return of the future 6 h given the past 24 h. We encode the future and past paths with their signatures of depth 4. Table 4 demonstrates that our proposed SigCWGAN outperforms the other baselines in terms of almost all the test metrics. The R^2 score of the RCGAN (0.3165) is slightly better than that of the SigCWGAN by 0.0155, whilst SigCWGAN achieves superior performance than the RCGAN in terms of other metrics, especially

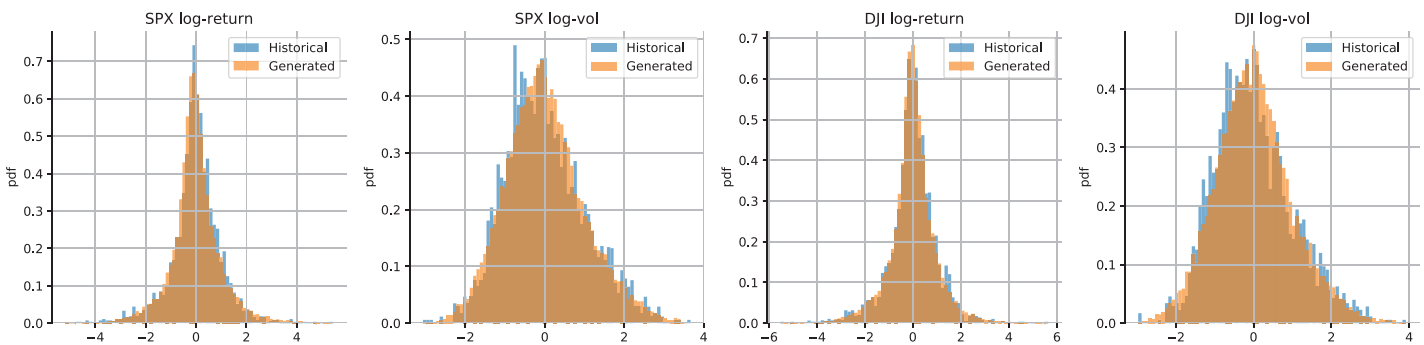

FIGURE 8 Comparison of the marginal distributions of the generated SigCWGAN paths and the SPX and DJI data. [Color figure can be viewed at wileyonlinelibrary.com]

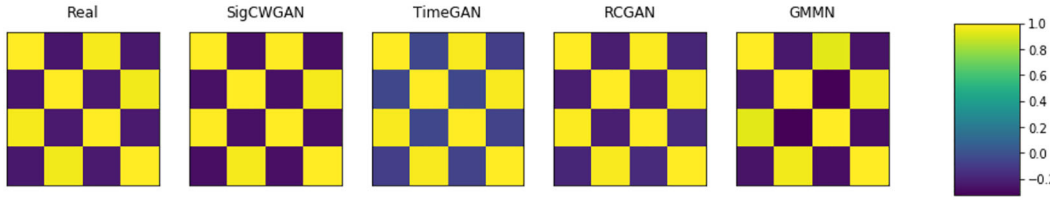

FIGURE 9 Comparison of real and synthetic cross-correlation matrices for SPX and DJI log-return and log-volatility data. On the far left, the real cross-correlation matrix from SPX and DJI data is shown. x/y-axis represents the feature dimension while the color of the (i, j)th block represents the correlation of $X_t^{(i)}$ and $X_t^{(j)}$. The color bar on the far right indicates the range of values taken. [Color figure can be viewed at wileyonlinelibrary.com]

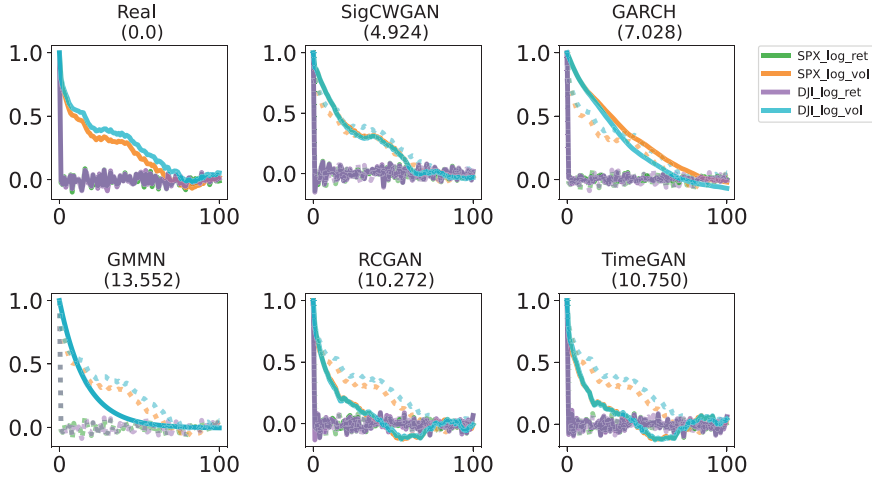

FIGURE 10 ACF plot for each channel on the SPX/DJI dataset. Here x-axis represents the lag value (with maximum lag equal to 100) and y-axis represent the corresponding auto-correlation. The length of real/generated time series used to compute the ACF is 1000. The number in the bracket under each model is the sum of the absolute difference between the correlation coefficients computed from real (dashed line) and generated (solid line) samples. [Color figure can be viewed at wileyonlinelibrary.com]

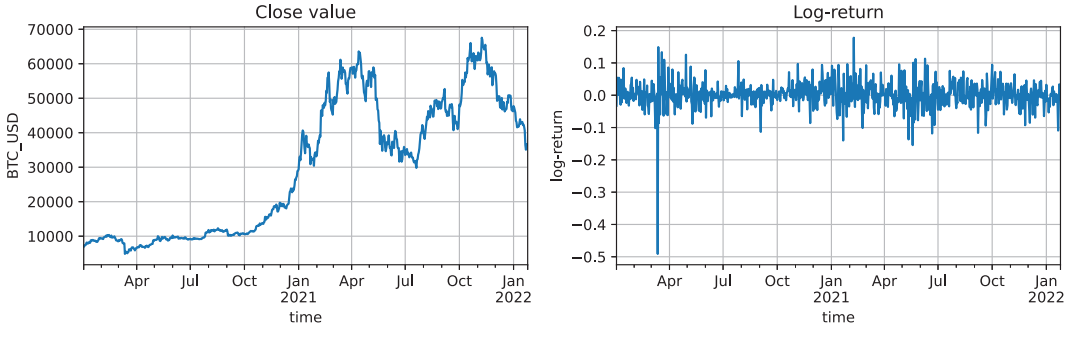

FIGURE 11 The evolution of the close value (left) and log return of BTC-USD from January 2021 to January 2023. [Color figure can be viewed at wileyonlinelibrary.com]

marginal distribution (2.0532 vs. 2.803). The better performance of the SigCWGAN to capture the temporal dependency is also verified by the additional results of the autocorrelation metric and the R^2-metric for different lag values is provided in Tables D.8 and D.9.

7 | CONCLUSION

In this paper, we developed the conditional Sig-Wasserstein GAN for time series generation based on the explicit approximation of W_1 metric using the signature features space. This eliminates the problem of having to approximate a costly critic/discriminator and, as a consequence, dramatically simplifies training. Our method achieves state-of-the-art results on both synthetic and empirical dataset.

Our proposed conditional Sig-Wasserstein GAN is proved to be effective for generating time series of a moderate dimension. However, it may suffer the curse of dimensionality caused by high path dimension. It might be interesting to explore how to combine SigCWGAN with the implicit generative model to learn the low-dimensional latent embedding and hence cope with the high-dimensional path case. Moreover, on the theoretical level, it is worthy of investigating the conditions, under which the W_1 metric on the signature space coincides with the Sig-W_1 metric.

ACKNOWLEDGMENTS

H.N. is supported by the EPSRC under the program Grant EP/S026347/1. H.N. and L.S. are supported by the Alan Turing Institute under the EPSRC Grant EP/N510129/1. All authors thank the anonymous referees for constructive feedback, which greatly improves the paper. Moreover, HN extends her gratitude to Siran Li, Terry Lyons, Chong Lou, Jiajie Tao, and Hang Lou for their helpful discussion.

DATA AVAILABILITY STATEMENT

The data that support the findings of this study are openly available in Conditional-Sig-Wasserstein-GANs repository at https://github.com/SigCGANs/Conditional-Sig-Wasserstein-GANs. These empirical data were derived from the following resources available in the public domain: (1) the Oxford-Man Institute's "realized library" https://realized.oxford-man.ox.ac.uk/data ;(2) https://github.com/David-Woroniuk/Historic_Crypto.

ORCID

Hao Ni https://orcid.org/0000-0001-5485-4376

ENDNOTES

[1] For any distribution $\mu^X \in \mathcal{P}(\mathbb{R}^{d\times W})$, one can construct a stochastic process $X : \Omega \to \mathbb{R}^{d\times W}$, such that Law$(X) = \mu^X$, see Dudley (1989, Proposition 9.1.2 and Theorem 13.1.1).

[2] The tensor power $E^{\otimes n}$ is defined based on the concept of the tensor product. Consider two vector spaces V and W over the same field F with basis B_V and B_W, respectively. The tensor product of V and W, denoted by $V \otimes W$, is a vector space consisting of basis $b \otimes b'$, where $b \in B_V$ and $b' \in B_W$ that is equipped with a bilinear map $\otimes$. Here $b \otimes b'$ can be regarded as a function $V \times W \to \mathbb{R}$, which maps every (v, w) to $\mathbf{1}_{v=b,w=b'}$. For any two elements $v = \sum_{b\in B_V} v_b\, b \in V$ and $w = \sum_{b'\in B_W} w_{b'}\, b' \in W$, then $v \otimes w = \sum_{b\in B_V, b'\in B_W} (v_b w_b)\, b \otimes b'$.

[3] One may refer Definition A.1, Appendix A for the p-variation metric of a path.

[4] The definition of infinite radius of convergence of expected signature can be found in Definition A.4 of Appendix A.

[5] To solely focus on the fitting of the conditional law of X_{future}, we use real past paths as the input data of train-on-synthetic experiment. In contrast, the input of train-on-synthetic in Yoon et al. (2019) is synthetic past path with the goal of assessing the unconditional generation of a long synthetic sequence in terms of its auto-regressive structure.

[6] Let $J = [s, t]$ be a closed bounded interval. A time partition of J is an increasing sequence of real numbers $\mathcal{D} = (t_0, t_1, \dots, t_r)$ such that $s = t_0 < t_1 < \cdots < t_r = t$. Let $|\mathcal{D}|$ denote the number of time points in $\mathcal{D}$, that is, $|\mathcal{D}| = r + 1$. $\Delta\mathcal{D}$ denotes the time mesh of $\mathcal{D}$, that is, $\Delta\mathcal{D} := \max_{i=0}^{r-1}(t_{i+1} - t_i)$.

REFERENCES

Assefa, S., Dervovic, D., Mahfouz, M., Balch, T., Reddy, P., & Veloso, M. (2020). Generating synthetic data in finance: Opportunities, challenges and pitfalls. *In Proceedings of the First ACM International Conference on AI in Finance*, 1–8.

Bellovin, S. M., Dutta, P. K., & Reitinger, N. (2019). Privacy and synthetic datasets. *Stanford Technology Law Review*, *22*, 1.

Boedihardjo, H., Diehl, J., Mezzarobba, M., & Ni, H. (2021). The expected signature of Brownian motion stopped on the boundary of a circle has finite radius of convergence. *Bulletin of the London Mathematical Society*, *53*(1), 285–299.

Boedihardjo, H., & Geng, X. (2015). The uniqueness of signature problem in the non-Markov setting. *Stochastic Processes and their Applications*, *125*(12), 4674–4701.

Buehler, H., Horvath, B., Lyons, T., Perez Arribas, I., & Wood, B. (2020). A data-driven market simulator for small data environments. *Available at SSRN 3632431*.

Chevyrev, I., & Kormilitzin, A. (2016). A primer on the signature method in machine learning. *arXiv preprint arXiv:1603.03788*.

Chevyrev, I., & Lyons, T. (2016). Characteristic functions of measures on geometric rough paths. *The Annals of Probability*, *44*(6), 4049–4082.

Chevyrev, I., & Oberhauser, H. (2022). Signature moments to characterize laws of stochastic processes. *The Journal of Machine Learning Research*, *23*(1), 7928–7969.

Cuchiero, C., Khosrawi, W., & Teichmann, J. (2020). A generative adversarial network approach to calibration of local stochastic volatility models. *Risks*, *8*(4), 101.

Daskalakis, C., Ilyas, A., Syrgkanis, V., & Zeng, H. (2017). Training GANs with optimism, In International Conference on Learning Representations 2018 Feb 15. *arXiv preprint arXiv:1711.00141*.

Daskalakis, C., & Panageas, I. (2018). The limit points of (optimistic) gradient descent in min-max optimization. *arXiv preprint arXiv:1807.03907*.

Donahue, C., McAuley, J. J., & Puckette, M. (2019). Adversarial audio synthesis. In *ICLR*.

Dudley, R. M. (1989). *Real analysis and probability*. Wadsworth & Brooks.

Engel, J., Agrawal, K. K., Chen, S., Gulrajani, I., Donahue, C., & Roberts, A. (2019). Gansynth: Adversarial neural audio synthesis, In International Conference on Learning Representations 2018 Sep 27. *ArXiv*, *abs/1902.08710*.

Esteban, C., Hyland, S. L., & RÃ¤tsch, G. (2017, Jun 8) Real-valued (medical) time series generation with recurrent conditional gans. arXiv preprint arXiv:1706.02633.

Farnia, F., & Ozdaglar, A.. 2020. Do GANs always have nash equilibria? In Proceedings of the 37th International Conference on Machine Learning (ICML'20), Vol. 119. JMLR.org, Article 284, 3029–3039.

Fawcett, T. (2002). *Problems in stochastic analysis: Connections between rough paths and non-commutative harmonic analysis* [PhD thesis, University of Oxford].

Fermanian, A. (2022). Functional linear regression with truncated signatures. *Journal of Multivariate Analysis*, *192*, 105031.

Fu, R., Chen, J., Zeng, S., Zhuang, Y., & Sudjianto, A. (2020). Time Series Simulation by Conditional Generative Adversarial Net. *International Journal of Mechanical and Industrial Engineering*, *14*(6), 458–471.

Genevay, A., Chizat, L., Bach, F., Cuturi, M., & Peyré, G. (2019). Sample complexity of sinkhorn divergences. In The 22nd international conference on artificial intelligence and statistics (pp. 1574–1583). PMLR.

Gierjatowicz, P., Sabate-Vidales, M., Siska, D., Szpruch, L., & Zuric, Z. (2022). Robust pricing and hedging via neural stochastic differential equations. *Journal of Computational Finance*, *26*(3).

Gulrajani, I., Ahmed, F., Arjovsky, M., Dumoulin, V., & Courville, A. (2017). Improved training of Wasserstein GANs. In Proceedings of the 31st International Conference on Neural Information Processing Systems (NIPS'17). Curran Associates Inc., Red Hook, NY, USA, 5769–5779.

Hambly, B., & Lyons, T. (2010). Uniqueness for the signature of a path of bounded variation and the reduced path group. *Annals of Mathematics*, *171*(1), 109–167.

He, K., Zhang, X., Ren, S., & Sun, J. (2015). Delving deep into rectifiers: Surpassing human-level performance on ImageNet classification. In *Proceedings of the IEEE international conference on computer vision* (pp. 1026–1034).

He, K., Zhang, X., Ren, S., & Sun, J. (2016). Deep residual learning for image recognition. In *Proceedings of the IEEE conference on computer vision and pattern recognition* (pp. 770–778).

Heber, G., Lunde, A., Shephard, N., & Sheppard, K. (2009). *Oxford-man institute's realized library. Version 0.3*. Oxford-Man Institute, University of Oxford.

Heusel, M., Ramsauer, H., Unterthiner, T., Nessler, B., & Hochreiter, S. (2017). GANs trained by a two time-scale update rule converge to a local nash equilibrium. In *Advances in neural information processing systems* (pp. 6626–6637).

Hyland, S., Esteban, C., & Rätsch, G. (2018). Real-valued (medical) time series generation with recurrent conditional GANs.

Karatzas, I., & Shreve, S. E. (1998). *Brownian motion*. Springer.

Kidger, P., Bonnier, P., Arribas, I. P., Salvi, C., & Lyons, T. (2019). Deep signature transforms. In *Advances in neural information processing systems* (pp. 3099–3109).

Kingma, D P., & Ba, J. (2015). Adam: A method for stochastic optimization, In proceedings of 3rd International Conference on Learning Representations, ICLR, San Diego, CA, USA, May 7–9, 2015, Conference.

Klüppelberg, C., Lindner, A., & Maller, R. (2004). A continuous-time GARCH process driven by a Lévy process: Stationarity and second-order behaviour. *Journal of Applied Probability*, *41*, 601–622.

Koochali, A., Dengel, A., & Ahmed, S. (2021). If You Like It, GAN It–Probabilistic Multivariate Times Series Forecast with GAN. *Engineering Proceedings*, *5*(1), 40. https://doi.org/10.3390/engproc2021005040

Koshiyama, A., Firoozye, N., & Treleaven, P. (2021). Generative adversarial networks for financial trading strategies fine-tuning and combination. *Quantitative Finance*, *21*(5), 797–813.

Levin, D., Lyons, T., & Ni, H. (2016). Learning from the past, predicting the statistics for the future, learning an evolving system. arXiv preprint arXiv:1309.0260.v6.

Li, S., & Ni, H. (2022). Expected signature of stopped Brownian motion on d-dimensional $C^{2,\alpha}$-domains has finite radius of convergence everywhere: $2 \leq d \leq 8$. *Journal of Functional Analysis*, *282*(12), 109447.

Li, Y., Swersky, K., & Zemel, R. (2015). Generative moment matching networks. In *International conference on machine learning* (pp. 1718–1727).

Lin, T., Jin, C., & Jordan, M. (2020). On gradient descent ascent for nonconvex-concave minimax problems. In *International conference on machine learning* (pp. 6083–6093). PMLR.

Liu, X., Xiao, T., Si, S., Cao, Q., Kumar, S., & Hsieh, C.-J. (2019). Neural SDE: Stabilizing neural ODE networks with stochastic noise. *arXiv preprint arXiv:1906.02355*.

Lucic, M., Kurach, K., Michalski, M., Gelly, S., & Bousquet, O. (2018). Are GANs created equal? a large-scale study. Advances in neural information processing systems, 31.

Lyons, T., & Ni, H. (2015). Expected signature of brownian motion up to the first exit time from a bounded domain. *The Annals of Probability*, *43*(5), 2729–2762.

Lyons, T. J., Caruana, M., & Lévy, T. (2007). *Differential equations driven by rough paths*. Springer.

Mazumdar, E. V., Jordan, M. I., & Sastry, S. S. (2019). On finding local Nash equilibria (and only local Nash equilibria) in zero-sum games. *arXiv preprint arXiv:1901.00838*.

Mertikopoulos, P., Papadimitriou, C., & Piliouras, G. (2018). Cycles in adversarial regularized learning. In *Proceedings of the twenty-ninth annual ACM-SIAM symposium on discrete algorithms* (pp. 2703–2717). SIAM.

Mescheder, L., Geiger, A., & Nowozin, S. (2018). Which training methods for gans do actually converge? In *International conference on machine learning (ICML)* (pp. 3481–3490). PMLR.

Ng, A. Y., & Jordan, M. I. (2002). On discriminative vs. generative classifiers: A comparison of logistic regression and naive Bayes. In *Advances in neural information processing systems* (pp. 841–848).

Ni, H., Szpruch, L., Sabate-Vidales, M., Xiao, B., Wiese, M., & Liao, S. (2021). Sig-Wasserstein GANs for time series generation. In *2nd ACM international conference on AI in finance*.

Passeggeri, R. (2020). On the signature and cubature of the fractional brownian motion for h>12. *Stochastic Processes and their Applications*, *130*(3), 1226–1257.
Ren, Y., Zhu, J., Li, J., & Luo, Y. (2016). Conditional generative moment-matching networks. In *Advances in neural information processing systems* (pp. 2928–2936).
Tsay, R. S. (2005). *Analysis of financial time series* (Vol. 543). John Wiley & Sons.
Tucker, A., Wang, Z., Rotalinti, Y., & Myles, P. (2020). Generating high-fidelity synthetic patient data for assessing machine learning healthcare software. *NPJ Digital Medicine*, *3*(1), 1–13.
Wiese, M., Bai, L., Wood, B., & Buehler, H. (2019). Deep hedging: Learning to simulate equity option markets. In Proceedings of the 33rd Conference on Neural Information Processing Systems (NeurIPS 2019), Vancouver, Canada.
Wiese, M., Knobloch, R., Korn, R., & Kretschmer, P. (2020). Quant GANs: Deep generation of financial time series. *Quantitative Finance*, *20*, 1–22.
Xie, Z., Sun, Z., Jin, L., Ni, H., & Lyons, T. (2017). Learning spatial-semantic context with fully convolutional recurrent network for online handwritten Chinese text recognition. *IEEE Transactions on Pattern Analysis and Machine Intelligence*, *40*(8), 1903–1917.
Yang, W., Lyons, T., Ni, H., Schmid, C., & Jin, L. (2022). *Developing the path signature methodology and its application to landmark-based human action recognition*. Stochastic Analysis, Filtering, and Stochastic Optimization, 431–464.
Yoon, J., Jarrett, D., & van der Schaar, M. (2019). Time-series generative adversarial networks. In *Advances in neural information processing systems* (pp. 5509–5519).

How to cite this article: Liao, S., Ni, H., Sabate-Vidales, M., Szpruch, L., Wiese, M., & Xiao, B. (2023). Sig-Wasserstein GANs for conditional time series generation. *Mathematical Finance*, 1–49. https://doi.org/10.1111/mafi.12423

APPENDIX A: PRELIMINARY

For the sake of precision, we start by introducing basic concepts around the signature of a path, which lays the foundation for our analysis on the signature approximation for Wasserstein-1 Distance. We complete this section by providing the proof of Lemma 4.3, which is essential for the derivation of the proposed Sig-W_1 metric.

A.1 | Signature of a path

We introduce the p-variation as a measure of the roughness of the path. For ease of notation, let J denote a compact time interval.

Definition A.1 (p-Variation). Let $p \geq 1$ be a real number. Let $X : J \to E$ be a continuous path. The p-variation of X on the interval J is defined by

$$||X||_{p,J} = \left[\sup_{D \subset J} \sum_{j=0}^{r-1} \left| X_{t_{j+1}} - X_{t_j} \right|^p \right]^{\frac{1}{p}}, \tag{A.1}$$

where the supremum is taken over any time partition of J, that is, $D = (t_1, t_2, \dots, t_r)$. [6]

Let $C^p(J, E)$ denote the set of all continuous paths mapping from J to E of finite p-variation. The larger the p-variation is, the rougher a path is. The compactness of the time interval J cannot

ensure the finite 1-variation of a continuous path in general. For example, Brownian motion has $(2+\varepsilon)$-variation a.s $\forall \varepsilon > 0$, but it has infinite p-variation a.s.$\forall p \in [1,2]$.

For each $p \geq 1$, the p-variation norm of a path $X \in C_p(J,E)$ is denoted by $||X||_{p-var}$ and defined as follows:

$$||X||_{p-var} = ||X||_{p,J} + \sup_{t\in J} ||X_t||.$$

Recall that π_n is the projection map from the tensor algebra element to its truncation up to level n. To differentiate with π_n, we also introduce another projection map $\Pi_n : T((E)) \to E^{\otimes n}$, which maps any $\mathbf{a} = (a_0, a_1, \dots, a_n, \dots)$ to its nth term a_n.

For concreteness, we state the decay rate of the signature for paths of finite 1-variation. However, there is a similar statement of the factorial decay for the case of paths of finite p-variation (Lyons et al., 2007).

Lemma A.2 (Factorial decay of the signature). *Let $X \in C_1(J,E)$. Then there exists a constant $C > 0$, such that for all $m \geq 0$,*

$$|\Pi_m(S(X))| \leq C\frac{|X|^m_{1-var}}{m!}.$$

Lemma A.3. *Let $\mathcal{K}$ denote a compact set of $\Omega_0([0,T],E)$. Then the range $S(\Omega_0([0,T],E))$ is a compact set on $T^p(E)$ endowed with l^p topology.*

Proof. The proof boils down to showing the continuity of the signature map S from $\Omega_0([0,T],E)$ with 1-variation norm to $\mathbf{T}^p(E)$ with l^p topology. Let $X, Y \in \Omega_0([0,T],E)$, which are controlled by the control function ω, for example, $\omega(s,t) := \max(|X_{s,t}|_{1-var}, |Y_{s,t}|_{1-var})$ for all $0 < s < t < T$. Let $|X_{[s,t]} - Y_{[s,t]}|_{1-var} \leq \epsilon\omega(s,t)$ for some $\epsilon \in \mathbb{R}^+$. Then by the continuity of the signature map in Theorem 3.10, Lyons et al. (2007), and the admissible norm l^1, it holds that for an integer $n \geq 1$,

$$|\Pi_m(S(X)) - \Pi_m(S(Y))|_1 \leq \epsilon\frac{\omega(0,T)^m}{\beta n!},$$

where $\beta = 2(1 + \sum_{r=3}^{\infty}(\frac{2}{r-2})^2)$. The direct calculation leads to that

$$||S(X) - S(Y)||_p \leq ||S(X) - S(Y)||_1 \leq \sum_{m=1}^{\infty}\left(\epsilon\frac{\omega(0,T)^m}{\beta m!}\right) = \frac{\epsilon}{\beta}\sum_{m=1}^{\infty}\left(\frac{\omega(0,T)^m}{m!}\right) < +\infty.$$

□

A.2 | Expected signature of stochastic processes

Definition A.4. Let X denote a stochastic process, whose signature is well defined almost surely. Assume that $\mathbb{E}[S(X)]$ is well-defined and finite. We say that $\mathbb{E}[S(X)]$ has infinite radius of convergence, if and only if for every $\lambda \geq 0$,

$$\sum_{n\geq 0}\lambda^n|\Pi_n(\mathbb{E}[S(X)])| < \infty.$$

A.3 | The signature Wasserstein-1 metric (Sig-W_1)

In the following, we provide the proof of Lemma 4.3.

Proof. Let $(e_I = e_{i_1} \otimes \cdots e_{i_n})_I$ be the canonical basis of $T((E))$. For any $a \in T((E))$, we write $a = (a_I)$, that is, $a = \sum_I a_I e_I$. Then $(e_I^* = e_{i_1}^* \otimes \cdots e_{i_n}^*)_{I=(i_1,\ldots,i_n)}$ is the basis of $T((E))^*$ and we can write $L = \sum_I l_I e_I^*$.

To prove Equation (11), we solve the constraint optimization of maximizing $\boldsymbol{L}a$ with the constraint $||a||_p = 1$ by the Lagrange multiplier method. W.l.o.g, we only prove the case for $L \neq 0$ as it is trivial for $\boldsymbol{L} = 0$, (when $L = 0$, $La \equiv 0$, $||\boldsymbol{L}||_q = 0$, and Equation 11 holds). More specifically, we solve the unconstrained optimization

$$\mathcal{L}(a, \lambda) := \sup_a |\boldsymbol{L}a| + \lambda\left(\sum_I |a_I|^p - 1\right),$$

where $\boldsymbol{L} \neq 0$.

The optimal (a^*, λ^*) is a solution to the below equations:

$$\frac{\partial \mathcal{L}}{\partial a_I} = (\text{sign}(a_I l_I) l_I + (\lambda(p|a_I|^{p-1}\text{sign}(a_I)))) = 0, \forall I$$

$$\frac{\partial \mathcal{L}}{\partial \lambda} = \sum_I |a_I|^p - 1 = 0.$$

Then we obtain that $a^* = (a_I^*)_I$ with $a_I^* = \text{sign}(l_I)\frac{|l_I|^{\frac{1}{p-1}}}{\left(\sum_I |l_I|^{p/(p-1)}\right)^{1/p}} = \text{sign}(l_I)\frac{|l_I|^{\frac{1}{p-1}}}{\left(\sum_I |l_I|^q\right)^{1/p}}$. Then it follows that

$$l_I a_I^* = |l_I| \cdot \frac{|l_I|^{\frac{1}{p-1}}}{\left(\sum_I |l_I|^q\right)^{1/p}} = \frac{|l_I|^q}{\left(\sum_I |l_I|^q\right)^{1/p}} \geq 0;$$

$$|La^*| = La^* = \sum_I l_I a_I^* = \frac{\sum_I |l_I|^q}{\left(\sum_I |l_I|^q\right)^{1/p}} = \left(\sum_I |l_I|^q\right)^{1-1/p} = \left(\sum_I |l_I|^q\right)^{1/q} = ||L||_q.$$

By Hôlder's inequality,

$$\sup_{||a||_p=1} |\boldsymbol{L}a| \leq \sup_{||a||_p=1} ||a||_{\text{p}} ||\boldsymbol{L}||_q = ||L||_q,$$

and the superum $||\boldsymbol{L}||_q$ is obtained when $a = a^*$. We complete the proof of Equation (11).

The proof of Equation (12) is similar to the above. We only need to show the supremum taken over $||L|| = 1$ is the same as that $||L|| \leq 1$. Again we only prove for $a \neq 0$ as the $a = 0$ case is trivial. Similarly to the above, when $L^*(a) := (l_I^*)$ with

$$l_I^* = \text{sign}(a_I)\frac{|a_l|^{\frac{1}{p-1}}}{\left(\sum_I |a_I|^q\right)^{1/p}}, \tag{A.2}$$

$L^*(a)$ attains the supremum $\sup_{||L||_q=1} L(a) = ||a||_p$ and $||L^*||_q = 1$. By Hôlder's inequality,

$$\sup_{||L||_q \le 1} |\boldsymbol{L}a| \le \sup_{||\boldsymbol{L}||_q \le 1} ||a||_p ||\boldsymbol{L}||_q \le ||a||_p. \tag{A.3}$$

As $\sup_{||\boldsymbol{L}||_q \le 1} La$ can not exceed $||a||_p$ and $\boldsymbol{L}^*(a) = ||a||_p$, it follows

$$\sup_{||L||_q \le 1} |\boldsymbol{L}(a)| = ||a||_p.$$

□

APPENDIX B: CONDITIONAL SIGNATURE WASSERSTEIN GANS

In this section, we provide the algorithmic details of the conditional signature Wasserstein GANs for practical applications.

B.1 | Path transformations

The core idea of SigCWGAN is to lift the time series to the signature feature as a principled and more effective feature extraction. In practice, the signature feature may often be accompanied with several of the following path transformations:

- Time jointed transformation (Definition 4.3, Levin et al., 2013);
- Cumulative sum transformation: it is defined to map every $(X_t)_{t=1}^T$ to $CS_t := \sum_{i=1}^t X_i, \forall t \in \{1, \dots, T\}$ and $CS_0 = \mathbf{0}$ (eq. (2.20) in Chevyrev & Kormilitzin, 2016).
- Lead-Lag transformation (eq. (2.8) in Chevyrev & Kormilitzin, 2016).
- Lag added transformation: The m-lag added transformation of $(X_t)_{t=1}^T$ is defined as follows: $\text{Lag}_m(X) = (Y_t)_{t=1}^{T-m}$, such that

$$Y_t = (X_t, \dots, X_{t+m}).$$

Although in our analysis on the Sig-W_1 metric, we use the time augmented path to embed the discrete time series X to a continuous path for the ease of the discussion. However, to use Sig-W_1 metric to differentiate two measures on the path space, the only requirement for the way of embeddings, a discrete time series to a continuous path is that this embedding needs to ensure the bijection between the time series and its signature. Therefore, in practice, we can choose other embedding to achieve that; for example, by applying the lead-lag transformation to time series, one can ensure the one-to-one correspondence between the time series and the signature.

B.2 | AR-FNN architecture

We give a detailed description of the AR-FNN architecture below. For this purpose, let us begin by defining the employed transformations, namely the parametric rectifier linear unit and the residual layer.

Definition B.1 (Parametric rectifier linear unit). The parametrized function $\phi_\alpha \in C(\mathbb{R}, \mathbb{R}), \alpha \geq 0$ defined as

$$\phi_\alpha(x) = \max(0, x) + \alpha \min(0, x)$$

is called *parametric rectifier linear unit* (*PReLU*).

Definition B.2 (Residual layer). Let $F : \mathbb{R}^n \to \mathbb{R}^n$ be an affine transformation and $\phi_\alpha, \alpha \geq 0$ a PReLU. The function $R : \mathbb{R}^n \to \mathbb{R}^n$ defined as

$$R(x) = x + \phi_\alpha \circ F(x)$$

where ϕ_α is applied component-wise, is called *residual layer*.

The AR-FNN is defined as a composition of PReLUs, residual layers, and affine transformations. Its inputs are the past p-lags of the d-dimensional process we want to generate as well as the d-dimensional noise vector. A formal definition is given below.

Definition B.3 (AR-FNN). Let $d, \bar{p} \in \mathbb{N}$, $A_1 : \mathbb{R}^{d(\bar{p}+1)} \to \mathbb{R}^{50}$, $A_4 : \mathbb{R}^{50} \to \mathbb{R}^d$ be affine transformations, $\phi_\alpha, \alpha \geq 0$ a PReLU and $R_2, R_3 : \mathbb{R}^{50} \to \mathbb{R}^{50}$ two residual layers. Then the function ArFNN $: \mathbb{R}^{d\bar{p}} \times \mathbb{R}^d \to \mathbb{R}^d$ defined as

$$\text{ArFNN}(x, z) = A_4 \circ R_3 \circ R_2 \circ \phi_\alpha \circ A_1(xz)$$

where xz denotes the concatenated vectors x and z, is called *autoregressive feedforward neural network* (*AR-FNN*).

The pseudocode of generating the next $\bar{q}$-step forecast using G^θ is given in Algorithm 2.

ALGORITHM 2 Pseudocode of generating the next q-step forecast using G^θ

Input: $x_{t-\bar{p}+1:t}, G_\theta$

Output: $\hat{x}_{t+1:t+\bar{q}}$

$\hat{x}_{\text{future}} \leftarrow$ a matrix of zeros of dimension $d \times \bar{q}$.

$\hat{x} \leftarrow$the concatenation of $x_{t-\bar{p}+1:t}$ and $\hat{x}_{\text{future}}$.

for $i = 1 : \bar{q}$ **do**

  We sample Z_i from the iid standard normal distribution.

  $\hat{x}_{t+i} = G(\hat{x}_{t+i-\bar{p}:t+i-1}, Z_i)$.

return $\hat{x}_{t+1:t+\bar{q}}$.

APPENDIX C: NUMERICAL IMPLEMENTATIONS

We use the following public codes for implementing the below three baselines:

- RCGAN: https://github.com/ratschlab/RGAN
- Time-GAN: https://github.com/jsyoon0823/TimeGAN
- GMMN: https://github.com/yujiali/gmmn

Additionally, we implement a conditional Wasserstein GAN (CWGAN) in the VAR(1) example: we perform the min-max optimization (2) where the discriminator is parametrized by the same neural network architecture as the generator, that is, a three-layer FNN. We ensure that the discriminator is 1-Lipschitz by adding a gradient penalty term introduced by Gulrajani et al. (2017).

For a fair comparison, we use the same neural network generator architecture, namely the three-layer AR-FNN described in Section B.2, for the SigCWGAN, TimeGAN, RCGAN, and GMMN. The TimeGAN and RCGAN discriminators take as inputs the conditioning time series $X_{1:\bar{p}}$ concatenated with the synthetic time series $X_{\bar{p}+1:\bar{p}+\bar{q}}$. Both discriminators use the AR-FNN as the underlying architecture. However, the first affine layer is adjusted such that the AR-FNN is defined as a function of the concatenated time series, that is, $\bar{p}+\bar{q}$ lags and not $\bar{p}$-lags as for the generator. Similarly, the MMD is computed by concatenating the conditioning and synthetic time series. In order to obtain the bandwidth parameter for computing the MMD of the GMMN, we benchmarked the median heuristic against using a mixture of bandwidths spanning multiple ranges as proposed in Li et al. (2015) and found latter to work best. In our experiments, we used three kernels with bandwidths 0.1, 1, 5.

All algorithms were optimized for a total of 1000 generator weight updates. The neural network weights were optimized by using the Adam optimizer (Kingma & Ba, 2015) and learning rates for the generators were set to 0.001. For the RCGAN and TimeGAN, we applied two time-scale updates (TTUR) (Heusel et al., 2017) and set the learning rate to 0.003. Furthermore, we updated the discriminator's weights two times per generator weight update in order to improve convergence of the GAN.

In our numerical experiments, to compute the signature for the SigCWGAN method, we choose to apply the following path transformations on the time series before computing the signatures: (1) we combine the path x_{past} with its cumulative sum transformed path, denoted by y_{past}, which is a $2d$-dimensional path; (2) we apply 1-lag added transformation on y_{past}; (3) it follows with the lead-lag transformation. The signature of such transformed path can well capture the marginal distributions, auto-correlations, and other temporal characteristics of the time-series data.

In the following, we describe the calculation of the test metrics precisely. Let $(X_t)_{t=1}^{T}$ denote a d-dimensional time series sampled from the real target distribution. We first extract the input–out pairs $(X_{t-\bar{p}+1:t}, X_{t+1:t+\bar{q}})_{t\in\mathcal{T}}$, where $\mathcal{T}$ is the set of time indexes. Given the generator G, for each input sample $(X_{t-\bar{p}+1:t})$, we generate one sample of the $\bar{q}$-step forecast $\hat{X}^{(t)}_{t+1,t+\bar{q}}$ (if G is not a conditional generator, we generate a sample of $\bar{q}$-step forecast $\hat{X}^{(t)}_{t+1,t+\bar{q}}$ without any conditioning variable.). The synthetic data generated by G are given by $(\hat{X}^{(t)}_{t+1,t+\bar{q}})_t$, which we use to compute the test metrics.

Metric on marginal distribution. Following Wiese et al. (2019), we use $(X_{t+1:t+\bar{q}})_{t\in\mathcal{T}}$ and $(\hat{X}^{(t)}_{t+1:t+\bar{q}})_{t\in\mathcal{T}}$ as the samples of the marginal distribution of the real data and synthetic data per each time step. For each feature dimension $i \in \{1, \dots, d\}$, we compute two empirical density functions based on the histograms of the real data and synthetic data, respectively, denoted by $\hat{df}^{i}_{r}$ and $\hat{df}^{i}_{G}$. Then the metric on marginal distribution of the true and synthetic data is given by

$$\frac{1}{d}\sum_{i=1}^{d}\left|\hat{df}^{i}_{r} - \hat{df}^{i}_{G}\right|_1.$$

Absolute difference of lag-1 auto-correlation. The auto-covariance of ith feature of the real data with lag value k is computed by

$$\rho_r^i(k) := \frac{1}{T-k}\sum_{t=1}^{T-k}(X_t^i - \bar{X}^i)(X_{t+k}^i - \bar{X}^i), \tag{C.1}$$

where $\bar{X}^i$ is the average of $(X_t^i)_{t=1}^T$.

For the synthetic data, we estimate the auto-covariance of ith feature with lag value k is computed by

$$\rho_G^i(k) := \frac{1}{|\mathcal{T}|}\sum_{t=1}^{|\mathcal{T}|}\hat{X}_{t+1}^{(t),i}\hat{X}_{t+k+1}^{(t),i} - \left(\frac{1}{|\mathcal{T}|}\sum_{t=1}^{|\mathcal{T}|}\hat{X}_{t+1}^{(t),i}\right)\left(\frac{1}{|\mathcal{T}|}\sum_{t=1}^{|\mathcal{T}|}\hat{X}_{t+k+1}^{(t),i}\right). \tag{C.2}$$

The estimator of the lag-1 auto-correlation of the real/synthetic data is given by $\frac{\rho_r^i(1)}{\rho_r^i(0)}/\frac{\rho_G^i(1)}{\rho_G^i(0)}$. The ACF score is defined to be the absolute difference of lag-1 auto-correlation given as follows:

$$\frac{1}{d}\sum_{i=1}^{d}\left|\frac{\rho_r^i(1)}{\rho_r^i(0)} - \frac{\rho_G^i(1)}{\rho_G^i(0)}\right|.$$

Metric on the correlation. We estimate the covariance of the ith and jth feature of time series from the true data as follows:

$$\mathrm{cov}_r^{i,j} = \frac{1}{T}\sum_{t=1}^{T}X_t^iX_t^j - \left(\frac{1}{T}\sum_{t=1}^{T}X_t^i\right)\left(\frac{1}{T}\sum_{t=1}^{T}X_t^j\right). \tag{C.3}$$

Similarly, we estimate the covariance of the ith and jth feature of time series from the synthetic data by

$$\mathrm{cov}_G^{i,j} = \frac{1}{|\mathcal{T}|}\frac{1}{q}\sum_{t=1}^{|\mathcal{T}|}\sum_{s=1}^{q}\hat{X}_{t+s}^{(t),i}X_{t+s}^{(t),j} - \left(\frac{1}{|\mathcal{T}|}\sum_{t\in\mathcal{T}}\hat{X}_{t+s}^{(t),i}\right)\left(\frac{1}{|\mathcal{T}|}\sum_{t\in|\mathcal{T}|}X_{t+s}^{(t),j}\right). \tag{C.4}$$

Thus the estimator of the correlation of the ith and jth feature of time series from the real/synthetic data are given by $\tau_r^{i,j} := \frac{\mathrm{cov}_r^{i,j}}{\sqrt{\mathrm{cov}_r^{i,i}\mathrm{cov}_r^{j,j}}}$ and $\tau_G^{i,j} := \frac{\mathrm{cov}_G^{i,j}}{\sqrt{\mathrm{cov}_G^{i,i}\mathrm{cov}_G^{j,j}}}$. Then the metric on the correlation between the real data and synthetic data is given by l_1 norm of the difference of two correlation matrices $(\tau_r^{i,j})_{i,j\in\{1,\ldots,d\}}$ and $(\tau_G^{i,j})_{i,j\in\{1,\ldots,d\}}$.

TRTR/TSTR R^2. We split the input–output pairs $(X_{t-\bar{p}+1:t}, X_{t+1})$ from the real data into the train set and test set. We apply the linear signature model on real training data $(X_{t-\bar{p}+1:t}, X_{t+1})$, validate it and compute the corresponding R^2 on the real test data (TRTR R^2). Then we apply the same linear signature model on the synthetic data $(X_{t-\bar{p}+1:t}, \hat{X}_{t+1})$, where $\hat{X}_{t+1}$ is simulated by the generator conditioning on the $X_{t-\bar{p}+1:t}$. We evaluate the trained model on the real test data and corresponding R^2 is called (TSTR R^2).

APPENDIX D: SUPPLEMENTARY NUMERICAL RESULTS

D.1 | VAR(1) dataset

We conduct the extensive experiments on VAR(1) with different hyper-parameter settings, that is, $d \in \{1, 2, 3\}$, $\sigma, \phi \in \{0.2, 0.5, 0.8\}$.

Test metrics of different models

We apply SigCWGAN, CWGAN, and the other above-mentioned methods on VAR(1) different set with various hyper-parameter settings. The summary of the test metrics of all models on d dimensional VAR(1) data for $d = 1, 2, 3$ can be found in Tables D.1–D.3, respectively.

Additionally, apart from Figure 5, the R^2 comparison, we provide the bar charts to compare the performance of different methods on the VAR data in terms of other test metrics in Figures D.1–D.4.

TABLE D.1 Numerical results of VAR(1) for $d = 1$.

	Temporal correlations		
Settings	$\phi = 0.2$	$\phi = 0.5$	$\phi = 0.8$
Metric on marginal distribution			
SigCWGAN	0.0124	0.0100	0.0069
CWGAN	**0.0070**	0.0085	0.0110
TimeGAN	0.0304	0.0307	0.0194
RCGAN	0.0187	**0.0065**	**0.0054**
GMMN	0.0096	0.0087	0.0073
Absolute difference of lag-1 autocorrelation			
SigCWGAN	**0.0124**	**0.0039**	0.0044
CWGAN	0.0614	0.0179	0.0109
TimeGAN	0.0495	0.0787	0.0100
RCGAN	0.0429	0.0124	**0.0029**
GMMN	0.0219	0.0248	0.0118
R^2 obtained from TSTR. (TRTR first row)			
TRTR	0.0457	0.2568	0.6434
SigCWGAN	0.0451	**0.2562**	**0.6431**
CWGAN	0.0338	0.2406	0.6269
TimeGAN	0.0432	0.2506	0.6365
RCGAN	0.0437	**0.2562**	0.6429
GMMN	**0.0452**	0.2539	0.6317
Sig-W_1 distance			
SigCWGAN	**0.0524**	**0.0476**	0.0393
CWGAN	0.0560	0.0584	0.0528
TimeGAN	0.0648	0.0641	0.0660
RCGAN	0.0546	0.0505	0.0437
GMMN	0.0540	0.0482	**0.0378**

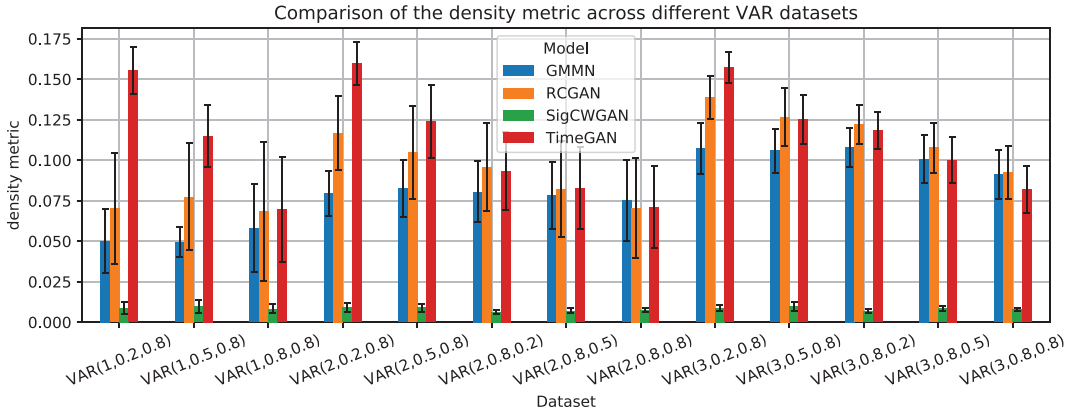

FIGURE D.1 Comparison of the performance on the density metric across all algorithms and benchmarks. [Color figure can be viewed at wileyonlinelibrary.com]

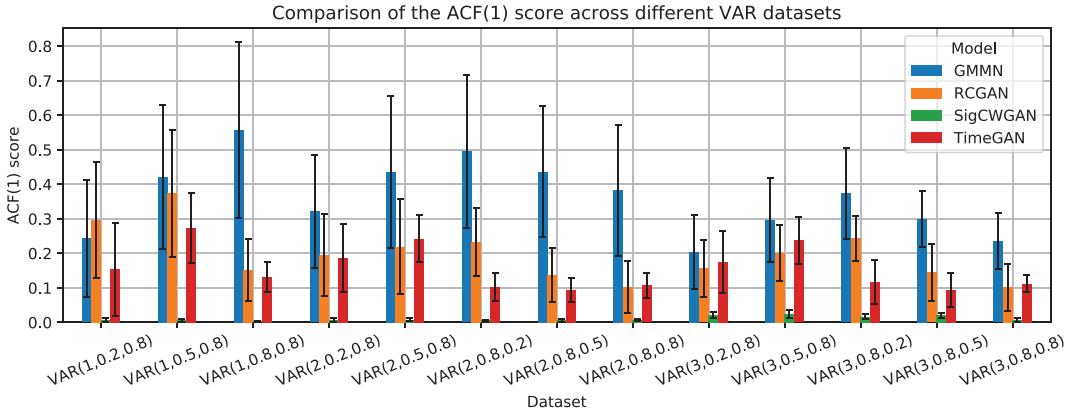

FIGURE D.2 Comparison of the performance on the absolute difference of lag-1 autocorrelation across all algorithms and benchmarks. [Color figure can be viewed at wileyonlinelibrary.com]

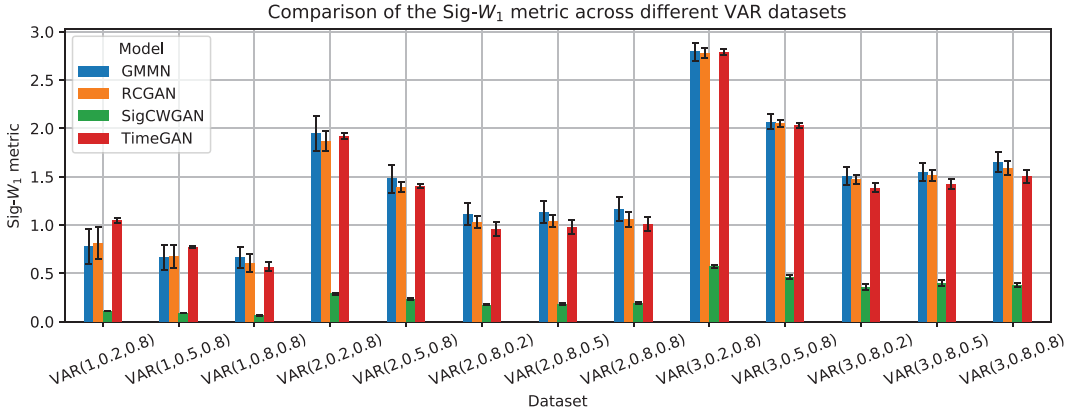

FIGURE D.3 Comparison of the performance on the Sig-W_1 metric across all algorithms and benchmarks. [Color figure can be viewed at wileyonlinelibrary.com]

TABLE D.2 Numerical results of VAR(1) for $d = 2$.

	Temporal correlations (fixing $\sigma = 0.8$)			Feature correlations (fixing $\phi = 0.8$)		
Settings	$\phi = 0.2$	$\phi = 0.5$	$\phi = 0.8$	$\sigma = 0.2$	$\sigma = 0.5$	$\sigma = 0.8$
Metric on marginal distribution						
SigCWGAN	0.0270	0.0122	**0.0084**	**0.0089**	**0.0088**	**0.0084**
CWGAN	0.0197	0.0134	0.0105	0.0154	0.0131	0.0105
TimeGAN	0.0270	0.0270	0.0173	0.0197	0.0164	0.0173
RCGAN	0.0120	0.0115	0.0091	0.0092	0.0104	0.0091
GMMN	**0.0098**	**0.0110**	0.0101	0.0104	0.0106	0.0101
Absolute difference of lag-1 autocorrelation						
SigCWGAN	**0.0069**	**0.0035**	**0.0054**	**0.0070**	**0.0062**	**0.0054**
CWGAN	0.0523	0.0198	0.0415	0.1138	0.0219	0.0415
TimeGAN	0.0484	0.0589	0.0110	0.0300	0.0345	0.0110
RCGAN	0.0401	0.0057	0.0294	0.0308	0.0373	0.0294
GMMN	0.0318	0.0505	0.0537	0.0868	0.0679	0.0537
L_1-norm of real and generated cross correlation matrices						
SigCWGAN	**0.0060**	0.0097	0.0122	**0.0040**	**0.0054**	0.0122
CWGAN	0.0820	0.1909	0.0048	0.0254	0.1592	0.0048
TimeGAN	0.0435	0.0243	0.0134	0.0401	0.0441	0.0134
RCGAN	0.0669	0.0286	0.0160	0.1614	0.1551	0.0160
GMMN	0.0066	**0.0006**	**0.0014**	0.0110	0.0103	**0.0014**
R^2 obtained from TSTR. (TRTR first row)						
TRTR	0.0420	0.2563	0.6467	0.6421	0.6444	0.6467
SigCWGAN	**0.0406**	**0.2552**	**0.6458**	**0.6416**	**0.6438**	**0.6458**
CWGAN	−0.0019	0.1573	0.5901	0.5850	0.6038	0.5901
TimeGAN	0.0337	0.2327	0.6298	0.6239	0.6344	0.6298
RCGAN	0.0295	0.2130	0.6166	0.5997	0.5984	0.6166
GMMN	0.0291	0.2296	0.6156	0.5823	0.5943	0.6156
Sig-W_1 distance						
SigCWGAN	**0.1913**	**0.1590**	**0.1190**	**0.2535**	**0.1235**	**0.1190**
CWGAN	0.2684	0.2702	0.2244	0.3487	0.2158	0.2244
TimeGAN	0.2057	0.2036	0.1372	0.2719	0.1445	0.1372
RCGAN	0.2116	0.2165	0.1657	0.3292	0.2386	0.1657
GMMN	0.2118	0.1831	0.1508	0.2977	0.1761	0.1508

Training stability

Figures D.5 and D.6 demonstrate the stability of the SigCWGAN optimization in terms of training iterations in contrast to other baselines, in particular two baselines involving the min–max game optimization.

D.2 | ARCH(p)

We implement extensive experiments on ARCH(p) with different p-lag values, that is, $p \in \{2, 3, 4\}$. We choose the optimal degree of signature 3. The numerical results are summarized in Table D.4. The best results among all the models are highlighted in bold.

TABLE D.3 Numerical results of VAR(1) for $d = 3$.

Settings	Temporal correlations (fixing $\sigma = 0.8$)			Feature correlations (fixing $\phi = 0.8$)		
	$\phi = 0.2$	$\phi = 0.5$	$\phi = 0.8$	$\sigma = 0.2$	$\sigma = 0.5$	$\sigma = 0.8$
Metric on marginal distribution						
SigCWGAN	0.0254	0.0112	**0.0077**	**0.0085**	**0.0076**	**0.0077**
CWGAN	0.0142	0.0148	0.0194	0.0210	0.0113	0.0194
TimeGAN	0.0222	0.0218	0.0193	0.0188	0.0110	0.0193
RCGAN	0.0112	0.0157	0.0121	0.0156	0.0159	0.0121
GMMN	**0.0098**	**0.0092**	0.0101	0.0176	0.0162	0.0101
Absolute difference of lag-1 autocorrelation						
SigCWGAN	**0.0137**	**0.0066**	**0.0054**	**0.0045**	**0.0025**	**0.0054**
CWGAN	0.0590	0.0242	0.1325	0.0864	0.0785	0.1325
TimeGAN	0.0554	0.0385	0.0374	0.1219	0.0879	0.0374
RCGAN	0.0864	0.0532	0.0217	0.1434	0.1303	0.0217
GMMN	0.0315	0.0584	0.0968	0.1183	0.1348	0.0968
L_1-norm of real and generated cross correlation matrices						
SigCWGAN	**0.0331**	**0.0498**	**0.0055**	**0.0532**	**0.0401**	**0.0055**
CWGAN	0.0628	0.2067	0.2812	0.4365	0.2071	0.2812
TimeGAN	0.6549	0.3619	0.1542	0.2644	0.3153	0.1542
RCGAN	0.4552	0.3441	0.0500	0.1448	0.4355	0.0500
GMMN	0.0811	0.1225	0.2405	0.3018	0.3883	0.2405
R^2 obtained from TSTR. (TRTR first row)						
TRTR	0.0420	0.2532	0.6509	0.6459	0.6485	0.6509
SigCWGAN	**0.0388**	**0.2490**	**0.6492**	**0.6446**	**0.6469**	**0.6492**
CWGAN	−0.0150	0.1770	0.5928	0.5462	0.5676	0.5928
TimeGAN	−0.0088	0.2039	0.6045	0.5600	0.6026	0.6045
RCGAN	0.0092	0.1994	0.5921	0.5064	0.5456	0.5921
GMMN	−0.0115	0.1683	0.5388	0.4899	0.4920	0.5388
Sig-W_1 distance						
SigCWGAN	**0.4289**	**0.3817**	**0.2374**	**0.2648**	**0.3999**	**0.2374**
CWGAN	0.4653	0.4173	0.3226	0.3875	0.4692	0.3226
TimeGAN	0.5030	0.4321	0.3087	0.3753	0.4415	0.3087
RCGAN	0.4751	0.4418	0.3034	0.4334	0.4859	0.3034
GMMN	0.4621	0.4159	0.3151	0.3946	0.4939	0.3151

D.3 | SPX and DJI dataset

We provide the supplementary results on the SPX and DJI dataset. The summary of test metrics of different models is given by Table D.5. The test metrics over the training process of each method on (1) SPX dataset and (2) SPX and DJI dataset can be found in Figures D.7 and D.8. The fitting of different models in terms of the cross-correlation matrix of the log-return and log-realized volatility of SPX is presented in Figure D.9 (see Tables D.6 and D.7).

D.4 | Bitcoin dataset

We provide the additional numerical results on the Bitcoin dataset as follows.

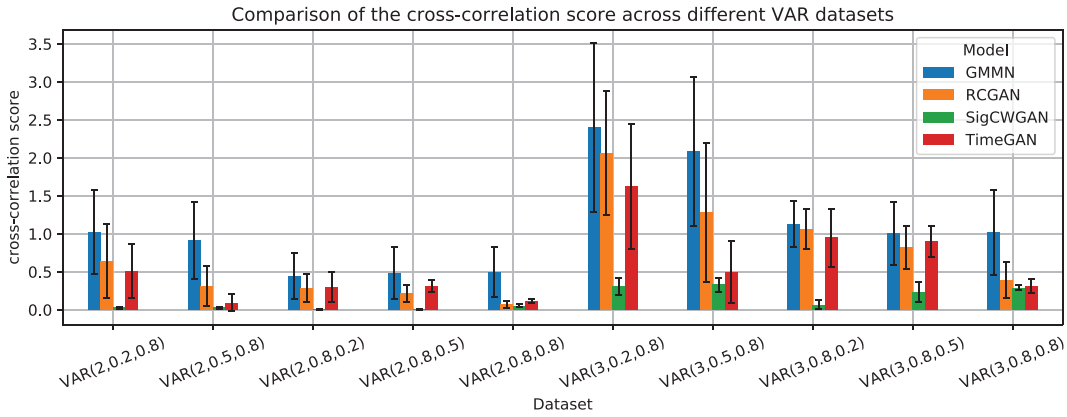

FIGURE D.4 Comparison of the performance on the cross-correlation metric across all algorithms and benchmarks. [Color figure can be viewed at wileyonlinelibrary.com]

TABLE D.4 Numerical results of the ARCH(p) datasets.

Settings	$p = 2$	$p = 3$	$p = 4$
Metric on marginal distribution			
SigCWGAN	0.00918	0.00880	**0.01142**
TimeGAN	0.02569	0.02119	0.2191
RCGAN	0.01069	0.01612	0.01182
GMMN	**0.00744**	**0.00783**	0.01259
Absolute difference of lag-1 autocorrelation			
SigCWGAN	**0.00542**	**0.00852**	**0.01106**
TimeGAN	0.01714	0.02401	0.03267
RCGAN	0.05372	0.01685	0.04879
GMMN	0.02056	0.00859	0.01441
L_1-norm of real and generated cross correlation matrices			
SigCWGAN	0.00462	**0.00546**	0.00489
TimeGAN	**0.00315**	0.06551	0.04408
RCGAN	0.01604	0.08823	**0.00235**
GMMN	0.04326	0.03930	0.01603
R^2 obtained from TSTR. (TRTR first row)			
TRTR	0.32168	0.32615	0.33305
SigCWGAN	**0.31623**	**0.31913**	**0.31642**
TimeGAN	0.30835	0.30556	0.30240
RCGAN	0.31146	0.30727	0.30924
GMMN	0.27982	0.28072	0.30742
Sig-W_1 distance			
SigCWGAN	**0.12210**	**0.14682**	**0.14098**
TimeGAN	0.20228	0.22761	0.23398
RCGAN	0.18781	0.20943	0.21876
GMMN	0.26797	0.26853	0.25811

TABLE D.5 Numerical results of the stocks datasets.

Data type	SPX	SPX + DJI
Metric on marginal distribution		
SigCWGAN	0.0142	**0.0093**
CWGAN	0.0111	0.0151
TimeGAN	0.0089	0.0156
RCGAN	**0.0088**	0.0140
GMMN	0.0107	0.0181
Absolute difference of lag-1 autocorrelation		
SigCWGAN	0.0302	0.0447
CWGAN	0.1617	0.0571
TimeGAN	**0.0180**	0.0232
RCGAN	0.0350	0.0515
GMMN	0.0273	**0.0106**
L_1-norm of real and generated cross correlation matrices		
SigCWGAN	0.0503	**0.0747**
CWGAN	**0.0131**	0.3908
TimeGAN	0.0793	0.5401
RCGAN	0.0654	0.3959
GMMN	0.0409	0.2103
R^2 obtained from TSTR. (TRTR first row)		
TRTR	0.3689	0.3731
SigCWGAN	**0.3576**	0.3466
CWGAN	0.2744	0.2694
TimeGAN	0.3551	**0.3602**
RCGAN	0.3037	0.3532
GMMN	0.3375	0.3368
Sig-W_1 distance		
SigCWGAN	**0.0985**	**0.1307**
CWGAN	0.1684	0.2881
TimeGAN	0.1265	0.2321
RCGAN	0.1462	0.2353
GMMN	0.1257	0.2448

TABLE D.6 R^2 metric (%) of the stock datasets for different lag values. In each cell, the left/right number are the result for the SPX data/ the SPX and DJI data, respectively.

Model lag	1	2	4	6	8
SigCWGAN	2.996, 7.948	**3.510**, 5.928	**3.801**, **7.439**	**3.944**, **9.103**	**5.534**, **10.742**
TimeGAN	5.955, 8.586	8.470, 9.925	10.838, 14.816	13.163, 20.139	16.922, 22.870
RCGAN	**2.788**, **7.190**	3.701, **5.425**	5.090, 9.407	6.033, 12.424	9.380, 16.599
GMMN	9.049, 7.384	11.275, 9.150	19.302, 14.466	25.832, 21.690	28.269, 24.778
GARCH	104.776, 100.749	99.359, 109.313	103.137, 109.53	102.939, 107.669	102.527, 104.779

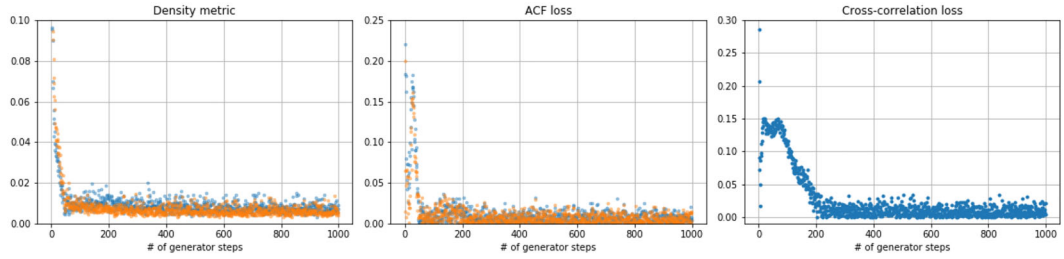

(a) SigCWGAN

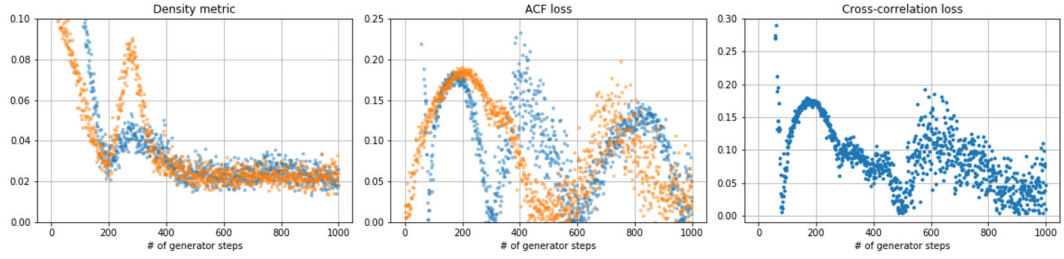

(b) TimeGAN

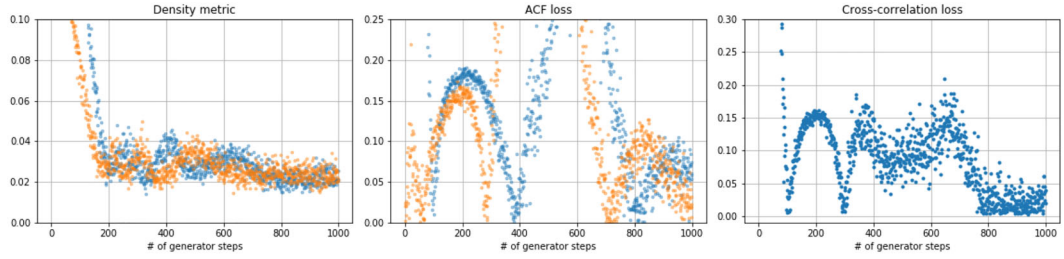

(c) RCGAN

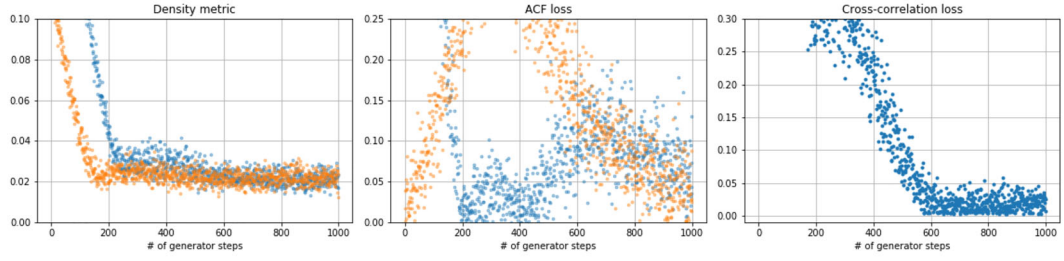

(d) GMMN

FIGURE D.5 Exemplary development of the considered distances and score functions during training for the two-dimensional VAR(1) model with autocorrelation coefficient $\phi = 0.8$ and covariance parameter $\sigma = 0.8$. The colors blue and orange indicate the relevant distance/score for each dimension. [Color figure can be viewed at wileyonlinelibrary.com]

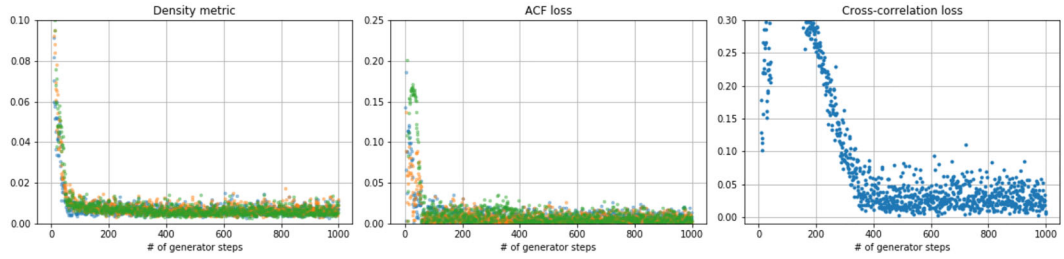

(a) SigCWGAN

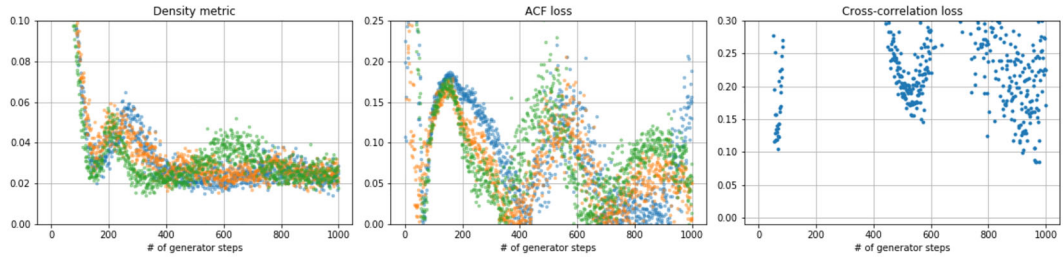

(b) TimeGAN

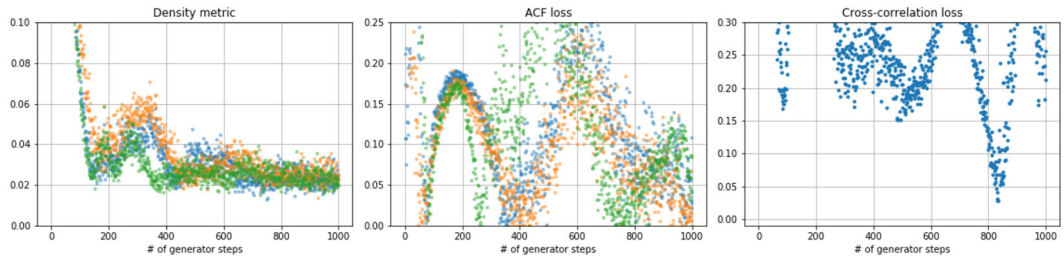

(c) RCGAN

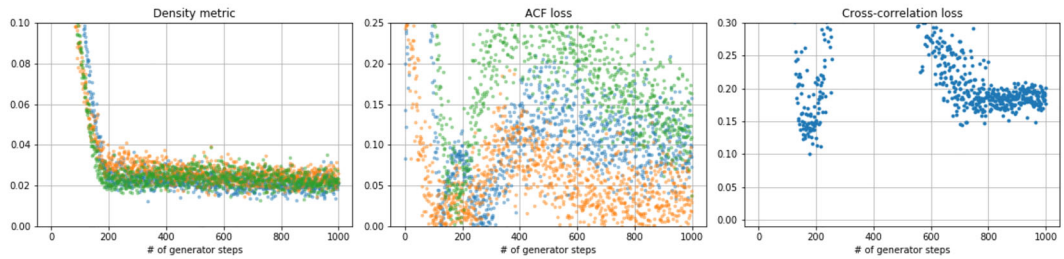

(d) GMMN

FIGURE D.6 Exemplary development of the considered distances and score functions during training for the three-dimensional VAR(1) model with autocorrelation coefficient $\phi = 0.8$ and covariance parameter $\sigma = 0.8$. The colors blue, orange, and green indicate the relevant distance/score for each dimension. [Color figure can be viewed at wileyonlinelibrary.com]

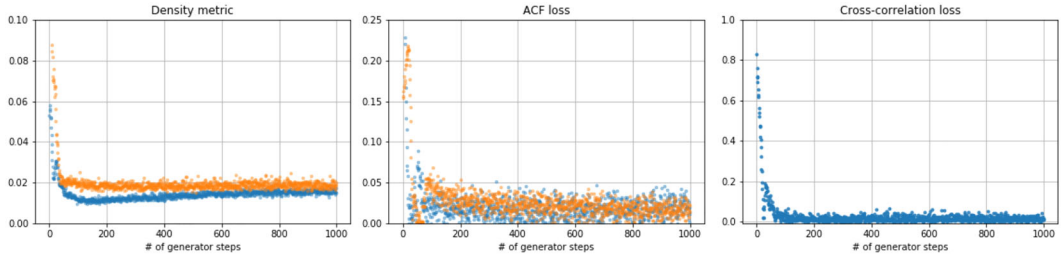

(a) SigCWGAN

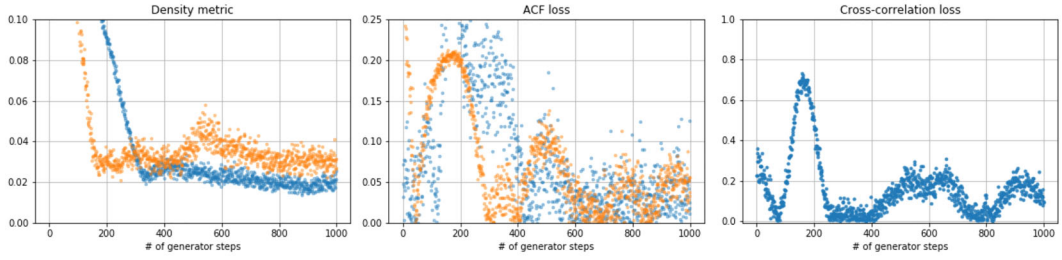

(b) TimeGAN

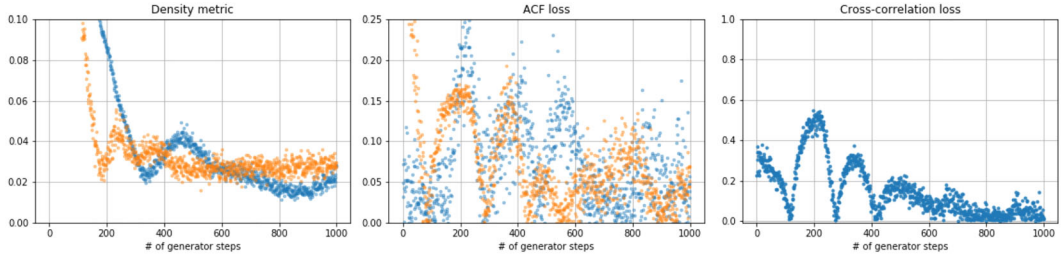

(c) RCGAN

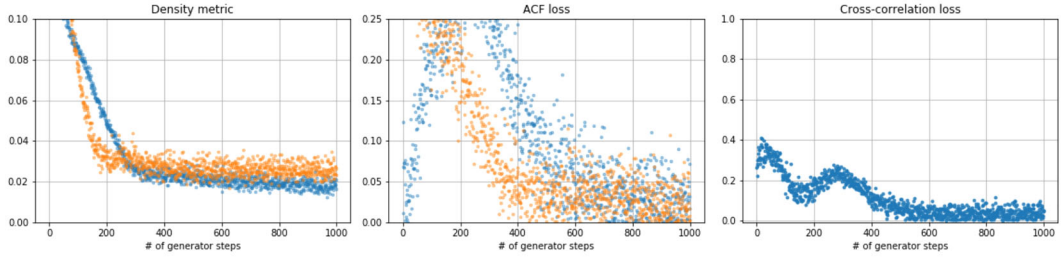

(d) GMMN

FIGURE D.7 Exemplary development of the considered distances and score functions during training for SPX data. [Color figure can be viewed at wileyonlinelibrary.com]

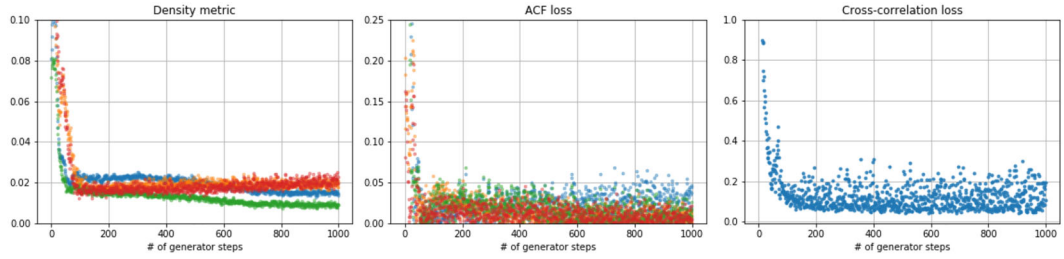

(a) SigCWGAN

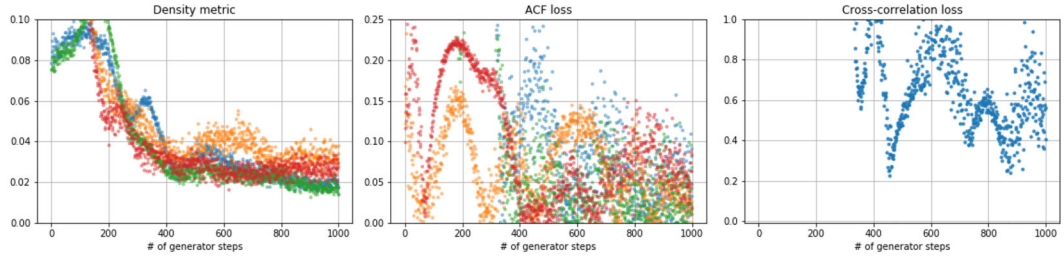

(b) TimeGAN

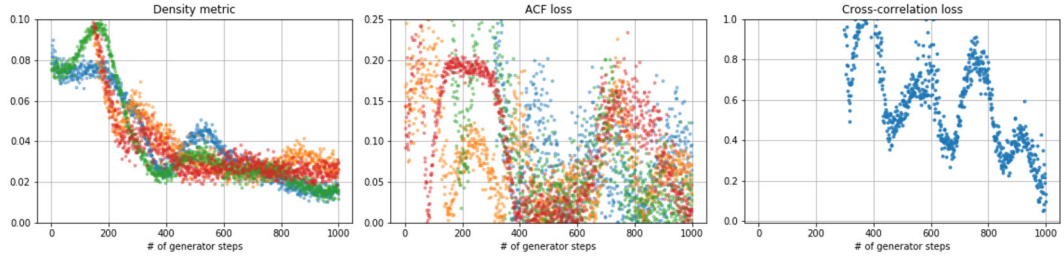

(c) RCGAN

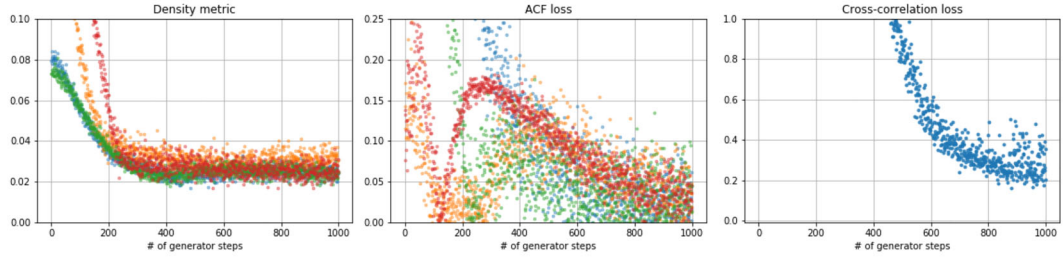

(d) GMMN

FIGURE D.8 ExemplARCHry development of the considered distances and score functions during training for SPX and DJI data. [Color figure can be viewed at wileyonlinelibrary.com]

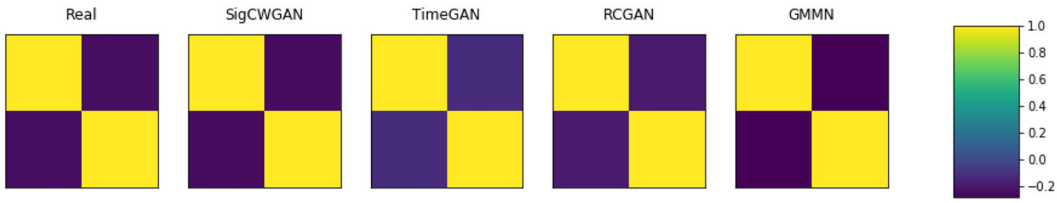

FIGURE D.9 Comparison of real and synthetic cross-correlation matrices for SPX data. On the far left, the real cross-correlation matrix from SPX log-return and log-volatility data is shown. x/y-axis represents the feature dimension while the color of the (i, j)th block represents the correlation of $X_t^{(i)}$ and $X_t^{(j)}$. The colorbar on the far right indicates the range of values taken. Observe that the historical correlation between log-returns and log-volatility is negative, indicating the presence of leverage effects, that is, when log-returns are negative, log-volatility is high. [Color figure can be viewed at wileyonlinelibrary.com]

TABLE D.7 Autocorrelation metric for the stock datasets for different lag values. In each cell, the left/right number are the result for the SPX data/the SPX and DJI data, respectively.

Model lag	1	2	3	4	5
SigCWGAN	0.01342, **0.01192**	0.02234, 0.02576	0.05744, **0.03592**	0.07389, 0.08646	0.12571, 0.1057
TimeGAN	0.05792, 0.03035	0.06070, 0.03182	0.06823, 0.09887	0.05735, 0.10609	**0.08387**, 0.15083
RCGAN	0.03362, 0.04075	0.03134, 0.03977	0.06692, 0.08859	**0.05641**, 0.07687	0.09089, 0.11083
GMMN	**0.01283**, 0.02676	**0.0177**, **0.0253**	**0.04293**, 0.06476	0.06740, **0.06952**	0.09589, **0.09906**
GARCH	0.4721, 0.4559	0.4661, 0.4741	0.6198, 0.6282	0.7292, 0.7312	0.8250, 0.8212

TABLE D.8 Autocorrelation metric for the BTC dataset for different lag values.

Model lag	1	2	3	4	5
SigCWGAN	0.0911	0.2814	0.3	0.3021	0.3028
TimeGAN	0.1203	0.2170	0.2312	0.2329	0.2568
RCGAN	0.0533	0.1486	0.15	0.1654	0.1751
GMMN	0.2093	0.3436	0.3448	0.3478	0.4333
GARCH	0.0872	0.1314	0.1378	0.1471	0.1501

TABLE D.9 R^2 metric (%) of the BTC dataset for different lag values.

Model lag	1	2	4	6
SigCWGAN	0.3320	0.2681	0.3843	0.3128
TimeGAN	0.7582	0.5962	0.6394	0.6018
RCGAN	0.3165	0.2191	0.2898	0.2261
GMMN	0.3904	0.3436	0.2583	0.3426
GARCH	123.77	87.35	96.47	117.34